THE JOURNAL OF BIOLOGICAL CHEMISTRY VOL. 291, NO. 37, pp. 19517–19531, September 9, 2016

Cannabinoid Receptor 2 Modulates Susceptibility to Experimental Cerebral Malaria through a CCL17-dependent Mechanism*

Received for publication, July 7, 2016 Published, JBC Papers in Press, July 29, 2016, DOI 10.1074/jbc.M116.746594

Judith Alferink[‡§¶1,2], Sabine Specht[‖1,3], Hannah Arends[‡1], Beatrix Schumak[‖4], Kim Schmidt[‖], Christina Ruland[§], Ramona Lundt[‡], Andrea Kemter[‡], Andrea Dlugos[§], Janina M. Kuepper[‖], Karola Poppensieker[‡], Matthias Findeiss[‡], Önder Albayram[‡4], David-M. Otte[‡], Janine Marazzi[**], Jürg Gertsch[**], Irmgard Förster[‡‡4], Wolfgang Maier[§§], Stefanie Scheu[¶¶], Achim Hoerauf[‖4], and Andreas Zimmer[‡4,5]

From the [‡]Institute of Molecular Psychiatry, Medical Faculty, and the [‡‡]Department of Immunology and Environment, Life and Medical Sciences Institute (LIMES), University of Bonn, 53127 Bonn, Germany, the [§]Department of Psychiatry, University of Münster, 48149 Münster, Germany, the [¶]Cluster of Excellence EXC 1003, Cells in Motion, 48149 Münster, Germany, the [‖]Institute of Medical Microbiology, Immunology, and Parasitology and the [§§]Department of Psychiatry, University Hospital Bonn, 53105 Bonn, Germany, the [**]Institute of Biochemistry and Molecular Medicine, University of Bern, 3012 Bern, Switzerland, and the [¶¶]Institute of Medical Microbiology and Hospital Hygiene, University of Düsseldorf, 40225 Düsseldorf, Germany

Cerebral malaria is a severe and often fatal complication of *Plasmodium falciparum* infection. It is characterized by parasite sequestration, a breakdown of the blood-brain barrier, and a strong inflammation in the brain. We investigated the role of the cannabinoid receptor 2 (CB2), an important modulator of neuroinflammatory responses, in experimental cerebral malaria (ECM). Strikingly, mice with a deletion of the CB2-encoding gene (*Cnr2*$^{-/-}$) inoculated with *Plasmodium berghei* ANKA erythrocytes exhibited enhanced survival and a diminished blood-brain barrier disruption. Therapeutic application of a specific CB2 antagonist also conferred increased ECM resistance in wild type mice. Hematopoietic derived immune cells were responsible for the enhanced protection in bone marrow (BM) chimeric *Cnr2*$^{-/-}$ mice. Mixed BM chimeras further revealed that CB2-expressing cells contributed to ECM development. A heterogeneous CD11b^{+} cell population, containing macrophages and neutrophils, expanded in the *Cnr2*$^{-/-}$ spleen after infection and expressed macrophage mannose receptors, arginase-1 activity, and IL-10. Also in the *Cnr2*$^{-/-}$ brain, CD11b^{+} cells that expressed selected anti-inflammatory markers accumulated, and expression of inflammatory mediators IFN-γ and TNF-α was reduced. Finally, the M2 macrophage chemokine CCL17 was identified as an essential factor for enhanced survival in the absence of CB2, because CCL17 × *Cnr2* double-deficient mice were fully susceptible to ECM. Thus, targeting CB2 may be promising for the development of alternative treatment regimes of ECM.

Cerebral malaria (CM)[6] is a life-threatening complication of *Plasmodium falciparum* infection and one of the leading causes of mortality worldwide (1–3). CM pathology is associated with a sequestration of parasitized red blood cells within the CNS microvasculature, which triggers an excessive inflammatory CNS response and an increase in blood-brain barrier permeability (1, 2). CM can be modeled in mice through inoculation with *Plasmodium berghei* ANKA (PbA)-infected red blood cells (1–8). Those mice develop severe neurological symptoms of ECM within 5–8 days after infection that lead to coma and death by days 7–9 (4). Disease pathogenesis is associated with a widespread activation of microglial cells, the production of inflammatory cytokines, and endothelial cell damage (1, 6). It was suggested that macrophages support pathogenic T cell responses in the CNS leading to the death of mice with experimental CM (ECM). Conversely, macrophages are also capable of mediating anti-parasite responses by clearance of parasites or production of IL-10, a cytokine shown to limit disease progression (9–11).

The endocannabinoid system plays a key role in immune modulation of the CNS by signaling via CB2 (12–19). It may therefore hold a therapeutic potential for the treatment of

* This study was supported by German Research Foundation (Deutsche Forschungsgemeinschaft (DFG)) Grant FOR926 (to J. A. and A. Z.); DFG EXC 1003, Grant FF-2014-01 Cells in Motion Cluster of Excellence, Münster, Germany (to J. A.); DFG Grants SCHE692/3-1 and SCHE692/4-1 (to S. Scheu); Strategic Research Fund of Heinrich Heine University Düsseldorf (to S. Scheu); DFG Grant SFB 704 (to I. F.); BONFOR intramural funding scheme of the Medical Faculty, Bonn University, Grants 2012-1-22 and 2013-1-29 (to J. K. and B. S.); intramural Münster IMF funding Grant I-DL121204 (to J. A. and A. D.); and intramural Münster IMF funding Grant I-ST111423 (to J. A.). The authors declare that they have no conflicts of interest with the contents of this article.

[1] These authors contributed equally to this work.

[2] To whom correspondence may be addressed: University of Münster, Department of Psychiatry, Albert-Schweitzer-Campus 1, 48149 Münster, Germany. Tel.: 49-251-8356663; Fax: 49-251-8356603; E-mail: Judith.alferink@ukmuenster.de.

[3] Present address: Institute of Laboratory Animal Science, Vetsuisse Faculty, University of Zurich, 8952 Schlieren, Switzerland.

[4] Members of the DFG EXC 1023 Cluster of Excellence ImmunoSensation (EXC 1023).

[5] To whom correspondence may be addressed: Institute of Molecular Psychiatry, University of Bonn, Sigmund Freud Str. 25, 53127 Bonn, Germany. Tel.: 49-228-6885302; Fax: 49-228-6885301; E-mail: neuro@uni-bonn.de.

[6] The abbreviations used are: CM, cerebral malaria; CB1 and CB2, cannabinoid receptor 1 and 2, respectively; ECM, experimental CM; BBB, blood-brain barrier; RBC, red blood cell; iRBC, infected RBC; CFSE, carboxyfluorescein diacetate succinimidyl ester; PbA, *P. berghei* ANKA; BM, bone marrow; 2-AG, 2-arachidonylglycerol; AA, arachidonic acid; GrzB, granzyme B; MMR, mannose macrophage receptor; MDSC, myeloid-derived suppressor cell; OVA, ovalbumin.

infectious CNS disorders. CB2 signaling affects various macrophage functions, such as antigen uptake, antigen presentation, and chemokine/cytokine production. For example, macrophages isolated from *Cnr2*$^{-/-}$ mice presented reduced T cell stimulatory potential *in vitro* compared with WT controls, indicating CB2-mediated alterations in antigen processing (20, 21). In addition, it was demonstrated that activation of CB2 negatively regulated IL-12p40 and NO production but enhanced IL-10 release in LPS-activated macrophages (22, 23).

In this study, we investigated the role of CB2 in ECM by using *Cnr2*$^{-/-}$ mice, mixed bone marrow (BM) chimeras, and a pharmacological approach. We could demonstrate that CB2 modulates susceptibility to ECM associated with anti-inflammatory macrophage effector responses. Our findings and the fact that the therapeutic application of the CB2 antagonist SR144528 conferred enhanced CM resistance in C57BL/6 mice provide the basis for the development of novel therapeutic strategies targeting CB2 for the treatment of ECM.

Results

Enhanced Protection of Cnr2$^{-/-}$ *Mice against ECM Is Mediated by Immune Cells*—We studied different components of the endocannabinoid system after PbA infection of C57BL/6 mice (20, 24). Expression of the cannabinoid receptor 2 (*Cnr2*) mRNA was markedly enhanced in the brain at day 6 after infection (Fig. 1*A*), whereas cannabinoid receptor 1 (*Cnr1*) expression remained unchanged ($2^{-\Delta Ct}$, control: 0.009 ± 0.00065; ECM: 0.009 ± 0.0003). Fatty acid amide hydrolase and diacylglycerol lipase β brain mRNA levels were not altered ($2^{-\Delta Ct}$, control: 0.0054 ± 0.0008; ECM WT: 0.0052 ± 0.0015). However, diacylglycerol lipase α, an enzyme involved in the biosynthesis of the endocannabinoid 2-arachidonylglycerol (2-AG), and monoacylglycerol lipase, an enzyme metabolizing 2-AG, were significantly increased (Fig. 1*B*). The enhanced expression of these enzymes suggested an increased turnover of 2-AG. We determined indeed similar 2-AG levels in PbA-infected and control mice, whereas arachidonic acid (AA) levels were higher, potentially reflecting 2-AG hydrolysis (Fig. 1*C*). Thus, brain 2-AG signaling via CB2 seems to be affected by PbA infection.

We found that PbA-infected WT mice developed severe ECM starting at day 5 and succumbed to ECM 24–48 h later (Fig. 1, *D* and *E*). In contrast, infected *Cnr2*$^{-/-}$ mice exhibited a diminished clinical score and an enhanced survival ($p < 0.0001$). Approximately 50% of the infected *Cnr2*$^{-/-}$ mice were protected from development of ECM and finally succumbed to hyperparasitemia and severe anemia after >20 days. This variability in survival points toward threshold effects influencing cerebral symptoms and survival of *Cnr2*$^{-/-}$ mice. Parasitemia in *Cnr2*$^{-/-}$ mice was similar to controls, indicating that a reduced parasite burden in the blood did not account for enhanced survival (Fig. 1*F*). However, attenuated ECM in *Cnr2*$^{-/-}$ mice was accompanied by a reduction of parasite-specific 18S RNA levels in the brain (Fig. 1*G*). The reduced 18S RNA in the presence of a comparable parasitemia in *Cnr2*$^{-/-}$ *versus* WT mice indicates a reduction in parasite sequestration in the brain (25). We therefore investigated the integrity of the blood-brain-barrier (BBB) by assessing the diffusion of Evans Blue into the brain (1, 2). In contrast to WT mice, infected *Cnr2*$^{-/-}$ brains displayed a reduced Evans Blue staining, indicative of an attenuated BBB disruption (Fig. 1*H*). Thus, the severity of PbA infection and incidence of ECM were significantly reduced in *Cnr2*$^{-/-}$ mice, which could account for the higher survival rate of these mice.

We next asked whether severity of ECM could also be modulated by pharmacological blockade of CB2 (26). PbA-infected C57BL/6 mice were treated daily with the CB2 antagonist SR144528. Most strikingly, these mice also showed an enhanced survival rate ($p = 0.0116$; Fig. 1*I*). These data demonstrate that the reduced ECM incidence in *Cnr2*$^{-/-}$ mice is due to a disrupted CB2 signaling rather than being a consequence of compensatory developmental changes. They also indicate a therapeutic potential of CB2 antagonists/inverse agonists.

To evaluate whether expression of CB2 on hematopoietically derived immune cells affects disease pathology, we reconstituted lethally irradiated WT mice with BM cells from *Cnr2*$^{-/-}$ (*Cnr2*$^{-/-}$ → WT) or WT (WT → WT) mice (Fig. 1*J*). *Cnr2*$^{-/-}$ → WT mice showed enhanced survival after PbA infection ($p < 0.01$), whereas all WT → WT chimeras succumbed to ECM. Thus, CB2 deficiency on immune cells, but not radioresistant CNS cells, protects against ECM.

Cnr2$^{-/-}$ *Myeloid-derived Cells Mediate Enhanced ECM Resistance in BM Chimeras*—Recruitment of immune cells to the brain is an important step in ECM pathology (7, 8). The absolute number of mononuclear brain-infiltrating cells was markedly reduced in *Cnr2*$^{-/-}$ mice at day 6 after PbA infection (Fig. 2*A*). Within this population, we observed increased percentages of CD11b$^+$ cells; >31% of cells that immigrated into the *Cnr2*$^{-/-}$ brain expressed CD11b, whereas <14% of CD11b$^+$ cells were found in WT brains (Fig. 2*B*). Equivalent percentages of CD4$^+$ T cells were found in the WT and *Cnr2*$^{-/-}$ brains (data not shown), whereas percentages of CD8$^+$ T cells were reduced in the brains of *Cnr2*$^{-/-}$ mice (Fig. 2*C*). We also found a reduced number of CD4$^+$ CD25$^+$ FoxP3$^+$ T cells in the *Cnr2*$^{-/-}$ brain, indicating that a T_{reg}-mediated mechanism does not contribute to disease protection in the absence of CB2 signaling (WT: $0.02 \times 10^4 \pm 0.01$; *Cnr2*$^{-/-}$: $0.01 \times 10^4 \pm 0.005$) (27).

We therefore focused on the reduced brain recruitment of CD8 T lymphocytes and the increased percentage of CD11b$^+$ myeloid-derived cells in the brains of infected *Cnr2*$^{-/-}$ mice, because both cell types are essential for acquisition and regulation of immunity in ECM (8, 28, 29). To determine whether CB2 expression in myeloid or lymphoid cells was required for susceptibility to ECM, we generated mixed BM chimeras by reconstitution of lethally irradiated WT mice with mixed BM from *Cnr2*$^{-/-}$ and RAG-2$^{-/-}$ mice (*Cnr2*$^{-/-}$ + RAG-2$^{-/-}$ → WT). In these mice, hematopoietically derived immune cells were CB2-deficient, with the exception of myeloid cells originating from RAG-2$^{-/-}$ BM cells (Fig. 2*D*). As controls, irradiated WT mice were reconstituted with *Cnr2*$^{-/-}$ (*Cnr2*$^{-/-}$ → WT) or WT BM cells (WT → WT). Again, infected *Cnr2*$^{-/-}$ → WT mice demonstrated enhanced survival in comparison with WT → WT chimeric mice ($p = 0.0089$). However, mixed BM chimeras (*Cnr2*$^{-/-}$ + RAG-2$^{-/-}$ → WT) showed

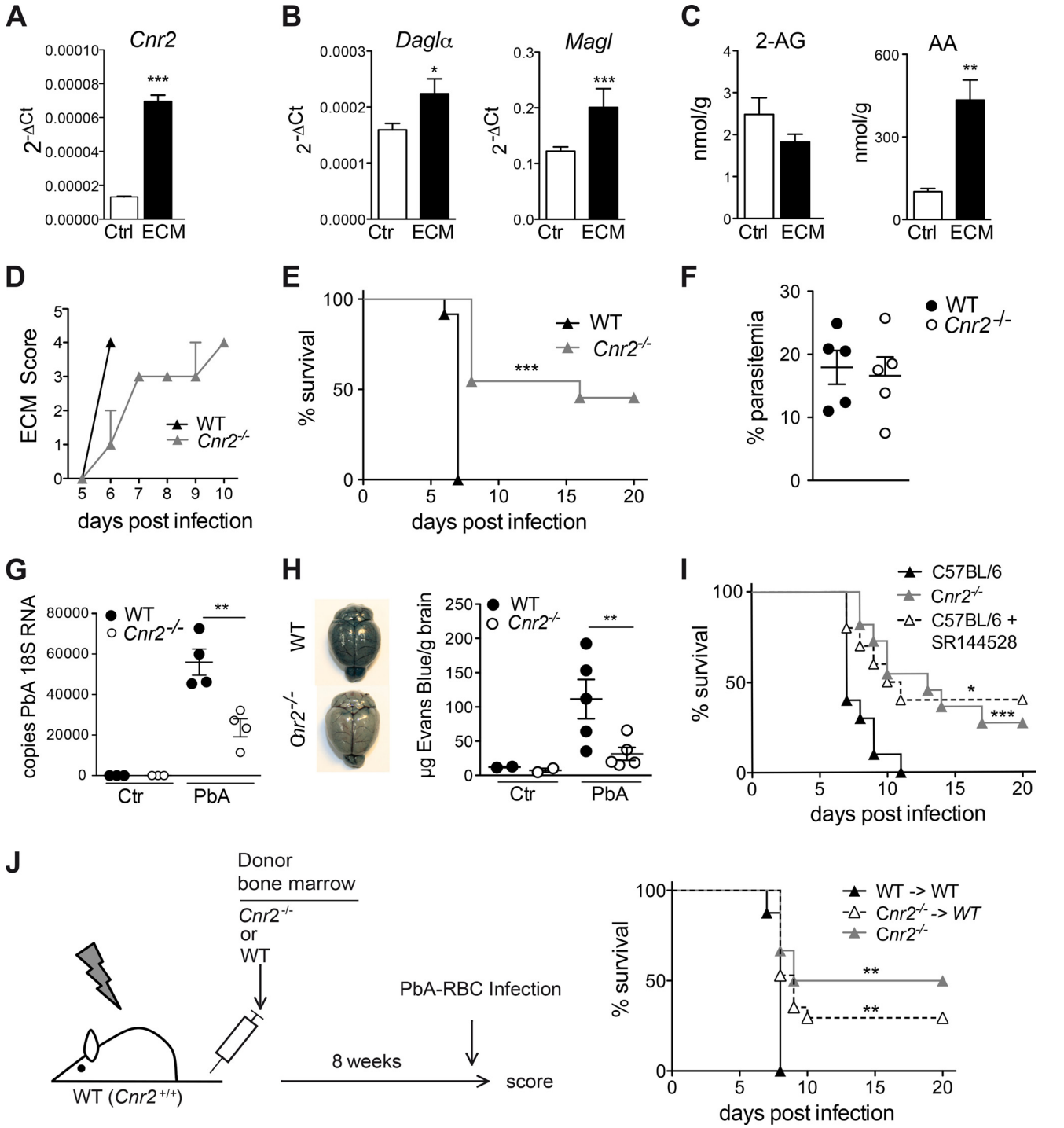

FIGURE 1. **Enhanced protection of *Cnr2*$^{-/-}$ mice from ECM is mediated by immune cells.** *A*, *Cnr2* mRNA expression in the brains of control and day 6 PbA-infected C57BL/6 mice. *B*, diacylglycerol lipase α (*Daglα*) and monoacylglycerol lipase mRNA expression in the brains of control and day 6 infected C57BL/6 mice (mean ± S.E. (*error bars*), $n = 3$–5 mice/group). *C*, levels of 2-AG and arachidonic acid (*AA*) in the brains of control or day 6 infected C57BL/6 mice (mean ± S.E. of nmol/g of total extracted brain, $n = 10$ mice/group). *D*, clinical score of infected mice. Clinical symptoms were scored daily as follows: 0, no clinical symptoms; 1, ruffled fur; 2, hunching; 3, wobbly gait; 4, limb paralysis; 5, convulsion; 6, coma. Representative data of one of at least five independent experiments are shown ($n = 10$–12 mice/group). *E*, survival of WT and *Cnr2*$^{-/-}$ mice after infection with PbA ($n = 10$–12 mice/group). *F*, peripheral parasitemia in WT and *Cnr2*$^{-/-}$ mice at day 6 after PbA infection as determined by Giemsa-stained thin blood smears. Representative data of one of three independent experiments are shown ($n = 5$ mice/group). *G*, parasite-specific 18S RNA expression in the brains of day 6 infected WT and *Cnr2*$^{-/-}$ mice, naive *Cnr2*$^{-/-}$ mice, and WT controls. *H*, reduced cerebral vascular leakage in PbA-infected *Cnr2*$^{-/-}$ mice, as assessed by blue staining of the brains of injected mice with Evans Blue on day 6 after PbA infection. The diagram shows mean ± S.E. µg of Evans Blue/g of brain tissue. *I*, survival of PbA-infected C57BL/6 mice treated daily with the CB2 antagonist SR144528 or vehicle and infected *Cnr2*$^{-/-}$ controls. Data from one of two representative experiments are shown ($n = 8$–12 mice/group). *J*, survival of PbA-infected BM chimeras and *Cnr2*$^{-/-}$ controls. Lethally irradiated WT mice were reconstituted with WT or *Cnr2*$^{-/-}$ BM cells and PbA-infected after successful reconstitution. One representative experiment of two independent experiments is shown ($n = 7$–12 mice/group). *, $p < 0.05$; **, $p < 0.01$; ***, $p < 0.001$.

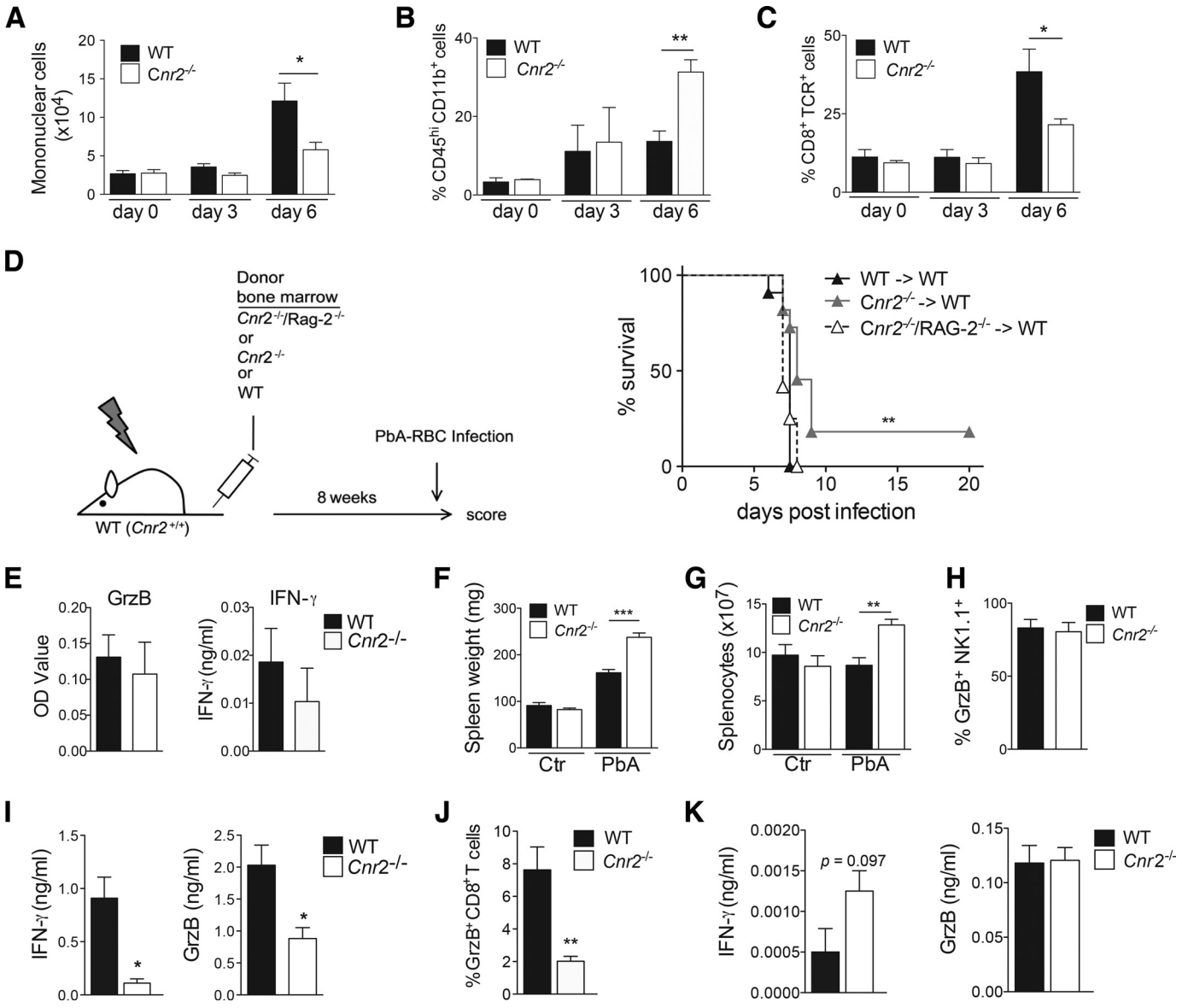

FIGURE 2. **CB2-deficient myeloid-derived cells mediate enhanced ECM resistance in BM chimeras.** *A*, reduced numbers of brain-infiltrating mononuclear cells in *Cnr2*$^{-/-}$ and WT mice at day 6 after PbA infection. Shown are mean numbers ± S.E. (*error bars*) of mononuclear cells isolated from the brains of the indicated mice at days 0, 3, and 6 after infection (n = 7–9 mice/group). *B*, enhanced percentages of brain-infiltrating CD11b$^+$ myeloid cells in day 6 infected *Cnr2*$^{-/-}$ mice as determined by flow cytometry. Shown are mean percentages ± S.E. of CD45^{hi} CD11b$^+$ cells in brain infiltrates isolated from the indicated mice at days 0, 3, and 6 after PbA infection (n = 7–9 mice/group). *C*, reduced percentages of brain-infiltrating CD8$^+$ TCR$^+$ cells in day 6 PbA-infected *Cnr2*$^{-/-}$ mice as determined by flow cytometry. Shown are mean percentages ± S.E. of CD8$^+$ TCR$^+$ cells (pregated for CD45^{hi} expression) in brain infiltrates isolated from the indicated mice at days 0, 3, and 6 after PbA infection (n = 7–9 mice/group). *D*, survival of mixed BM chimeric mice after PbA infection. BM chimeras were generated by reconstitution of lethally irradiated WT mice with BM cells from WT mice, *Cnr2*$^{-/-}$ mice, or mixed BM from *Cnr2*$^{-/-}$ and RAG-2$^{-/-}$ mice. One representative experiment of two independent experiments is shown (n = 8–10 mice/group). *E*, equivalent IFNγ and GrzB production by MACS-purified CD8$^+$ T cells from day 6 PbTg OVA-infected WT or *Cnr2*$^{-/-}$ mice (mean ± S.E., n = 5–6 mice/group). CD8$^+$ T cells were restimulated with 1 μM SIINFEKL peptide-loaded antigen-presenting cells from day 6 PbTg OVA-infected RAG-2$^{-/-}$ mice. Supernatants were analyzed for IFNγ and GrzB with ELISA. *F*, weight of spleens from WT or *Cnr2*$^{-/-}$ controls or at day 6 after PbA infection (mean ± S.E., n = 5–8 mice/group). *G*, number of spleen cells in WT or *Cnr2*$^{-/-}$ control mice or at day 6 after PbA infection (mean ± S.E., n = 8–10 mice/group). *H*, percentages of GrzB$^+$ NK1.1$^+$ cells in WT or *Cnr2*$^{-/-}$ spleens at day 6 after infection as determined by flow cytometry (mean ± S.E., n = 6–8 mice/group). *I*, IFN-γ and GrzB production by whole spleen cells from WT and *Cnr2*$^{-/-}$ mice 6 days after PbTg OVA infection. Spleen cells were restimulated with 1 μM SIINFEKL peptide overnight, and supernatants were analyzed by ELISA (mean ± S.E., n = 6 mice/group). *J*, percentages of GrzB$^+$ CD8$^+$ TCR$^+$ T cells in WT or *Cnr2*$^{-/-}$ spleens at day 6 after infection with PbTg OVA as determined by flow cytometry. Diagram shows percentages of cells (mean ± S.E., n = 6 mice/group). *K*, IFN-γ and GrzB production by MACS-purified spleen-isolated CD8$^+$ T cells from day 6 PbTg OVA-infected WT or *Cnr2*$^{-/-}$ mice. CD8$^+$ T cells were restimulated with 1 μM SIINFEKL peptide-loaded C57BL/6 dendritic cells, and supernatants were analyzed for IFN-γ and GrzB production (mean ± S.E., n = 4 mice/group).*, $p < 0.05$; **, $p < 0.01$; ***, $p < 0.001$.

100% mortality (Fig. 2*D*). These data point toward a contribution of CB2-expressing myeloid cells to the enhanced susceptibility to ECM. To analyze a possible role of CB2 in modulating CD8 T cell responses in this model, we investigated Th1 responses and cytotoxicity in *Cnr*2$^{-/-}$ and WT T cells (Fig. 2*E*). IFN-γ and granzyme B (GrzB) production was equivalent in *Cnr*2$^{-/-}$ and WT CD8$^+$ T cells when stimulated with cognate peptide-loaded spleen-derived DCs from infected RAG-2$^{-/-}$ mice, indicating that CB2 may not have a major CD8$^+$ T cell intrinsic function under these conditions.

Impact of CB2 Deficiency on the T, B, and NK Cell Compartment in the Spleen after PbA Infection—Next, we investigated immune responses in the spleens of infected *Cnr2*$^{-/-}$ and WT mice. *Cnr2*$^{-/-}$ spleens exhibited increased weight and total splenic cell numbers at day 6, indicating an altered cellular composition (Fig. 2, *F* and *G*). Flow cytometry determined that CD4$^+$ and CD8$^+$ T cells, as well as B220$^+$ CD11c$^-$ B cells, were present in equivalent numbers in the spleens of infected WT and *Cnr2*$^{-/-}$ mice (CD4$^+$ T cells in WT: $17.65 \times 10^6 \pm 5.3$ *versus* *Cnr2*$^{-/-}$: $18.79 \times 10^6 \pm 4.0$; CD8$^+$ T cells in WT: $10.94 \times 10^6 \pm 7.18$ *versus* *Cnr2*$^{-/-}$: $9.65 \times 10^6 \pm 4.8$; B220$^+$ CD11c$^-$ B cells in WT: $51.8 \times 10^6 \pm 39.9$ *versus* *Cnr2*$^{-/-}$: $53.5 \times 10^6 \pm 33.5$). No differences in NK cell numbers and percentages were found in the spleens from day 6 infected WT and *Cnr2*$^{-/-}$ mice (percentage of NK1.1 cells in WT: 0.97 ± 0.2 *versus* *Cnr2*$^{-/-}$: 0.75 ± 0.3; number of NK1.1 cells in WT: $1.6 \times 10^6 \pm 0.3$ *versus* *Cnr2*$^{-/-}$: $2.1 \times 10^6 \pm 1.0$). Equivalent percentages of GrzB-producing NK cells in infected mice further suggested that NK cells may not play a central role in immune protection against ECM in *Cnr2*$^{-/-}$ mice (Fig. 2*H*). We next investigated whether parasite-specific CD8$^+$ T cell responses, which are required in ECM induction (30, 31), were altered in *Cnr2*$^{-/-}$ mice. *S*plenocytes isolated from *Cnr2*$^{-/-}$ and WT mice were isolated at day 6 after infection with an OVA-transgenic parasite strain. *Cnr2*$^{-/-}$ splenocytes produced lower levels of IFN-γ and GrzB after restimulation with the SIINFEKL peptide when compared with WT splenocytes (Fig. 2*I*). Also, reduced percentages of GrzB$^+$ CD8$^+$ T cells in spleen cultures of *Cnr2*$^{-/-}$ mice indicated diminished splenic anti-parasitic T cell responses in the infected *Cnr2*$^{-/-}$ mice (Fig. 2*J*). In contrast, MACS-purified CD8$^+$ T cells from the spleens of infected *Cnr2*$^{-/-}$ mice produced these factors equivalently to WT CD8$^+$ T cells when restimulated with peptide presented by CB2-competent antigen-presenting cells (Fig. 2*K*). Thus, CB2 does not affect CD8 T cell function in ECM in a cell-intrinsic way.

CB2 Does Not Affect Antigen Presentation Capacities of BM DCs but Polarization of BM Macrophages in Vitro—To characterize CD11b$^+$ myeloid cells in *Cnr2*$^{-/-}$ mice in more detail, we first analyzed dendritic cells and macrophages generated from the BM of *Cnr*2$^{-/-}$ and WT mice. GM-CSF-generated *Cnr*2$^{-/-}$ BM DCs induced equivalent OT-II T cell responses when compared with WT BM DCs, as represented by proliferation, IFN-γ release, and GrzB production (Fig. 3, *A* and *B*). These data indicate that CB2 does not affect basic T cell priming properties of BM DCs. M-CSF-generated CD11b$^+$ BM macrophages from *Cnr2*$^{-/-}$ mice expressed enhanced Ym1 and arginase-1 (Arg-1) mRNA levels under IL-4-stimulatory conditions (Fig. 3*C*). They also exhibited enhanced expression of mannose macrophage receptors (MMRs) and secreted reduced levels of the pro-inflammatory cytokines TNF and IL-6 (Fig. 3, *D* and *E*), pointing toward anti-inflammatory properties of these cells (32).

Enhanced Numbers of Macrophages and Neutrophils in the Spleens of Cnr2$^{-/-}$ *Mice after PbA Infection*—In a next step, we investigated myeloid cell responses *in vivo* in infected *Cnr2*$^{-/-}$ and WT mice. In the blood, numbers of CD11b$^+$ CD11c$^-$ cells and Ly6G^{hi} neutrophils increased equivalently in *Cnr*2$^{-/-}$ and WT mice (Fig. 3*F*). In addition, comparable numbers of CD11c^{hi} MHC II$^+$ DCs were found at all time points after infection with equal proportions of conventional DCs (CD11b$^+$ CD11c$^+$, CD4$^+$ CD11c$^+$ DCs, and CD8$^+$ CD11c$^+$ DCs) as well as B220$^+$ plasmacytoid DCs (Fig. 3*G*).

However, in the splenic red pulp of infected *Cnr2*$^{-/-}$ mice, CD11b expression was markedly increased at day 6 after infection when compared with WT controls (Fig. 4*A*). Flow cytometry further verified enhanced percentages of CD11b$^+$ cells in the spleens of *Cnr2*$^{-/-}$ mice at this time point (Fig. 4*B*). Because CD11b is expressed on several myeloid cell types comprising macrophages, neutrophils, and DCs, we further characterized CD11b-expressing cells in *Cnr2*$^{-/-}$ mice (33–35). Higher percentages of CD11b$^+$ cells that were negative for CD11c accumulated in the spleens of infected *Cnr*2$^{-/-}$ mice, indicating that these cells do not exclusively represent CD11b-expressing DC subsets (Fig. 4*C*). Rather, numbers of CD11c^{hi} DCs decreased equally in the spleens of both mouse strains after infection (Fig. 4*D*). Furthermore, we identified no differences in the percentages of conventional and plasmacytoid DCs in WT *versus* *Cnr*2$^{-/-}$ mice at day 6 after infection (Fig. 4*E*). However, counts of CD11b$^+$ Ly6G^{hi} neutrophils markedly increased at this time point of infection in *Cnr*2$^{-/-}$ mice but not in WT mice (Fig. 4*F*). We further investigated whether increased numbers of CD11b$^+$ cells in the *Cnr*2$^{-/-}$ spleen also comprise macrophages by utilizing previously published gating strategies (36) (Fig. 4*G*). Red pulp macrophages (CD11b^{lo} F4/80$^+$ CD169^{lo} MHC II^{lo}), marginal zone macrophages (F4/80$^-$ CD11b$^-$ MARCO$^+$; *MMs*) and a subset of CD11b$^+$ F4/80^{hi} CD169^{lo} MHC-II^{lo} cells accumulated in the spleens of infected *Cnr*2$^{-/-}$ mice, with the exception of metallophilic marginal zone macrophages (F4/80$^-$ CD11b$^-$ CD169$^+$; *MMMs*) (Fig. 4*G*). These data suggest that accumulated CD11b$^+$ cells in *Cnr*2$^{-/-}$ *versus* WT spleens contain macrophages as well as neutrophils.

CD11b$^+$ *Cells in the Spleens of Infected Cnr2*$^{-/-}$ *Mice Exhibit an Anti-inflammatory Phenotype and Function*—We next investigated the phenotypic and functional profiles of splenic CD11b$^+$ cells in PbA-infected *Cnr*2$^{-/-}$ and WT mice. At day 6 after infection, CD11b$^+$ cells in the *Cnr2*$^{-/-}$ spleen exhibited enhanced expression of MMRs and Arg-1 activity (Fig. 5, *A* and *B*). Furthermore, isolated *Cnr*2$^{-/-}$ CD11b$^+$ cells secreted higher amounts of the anti-inflammatory cytokine IL-10 at this time point, suggesting that these cells exerted protective functions in *Cnr*2$^{-/-}$ mice after PbA infection (Fig. 5*C*).

To clarify the identity of IL-10-producing CD11b$^+$ cells in *Cnr2*$^{-/-}$ mice, we measured cytokine release in DCs, neutrophils, and macrophages isolated from the spleens of PbA-infected mice. We found no difference in the percentages of TNF- and IL-10-producing CD11c^{hi} MHC-II$^+$ DCs in the spleens of day 6 infected *Cnr2*$^{-/-}$ and WT mice *in vitro* and an equivalent increase of TNF$^+$ DCs after LPS restimulation of these cells (Fig. 5*D*). However, Ly6G$^+$ cells *bona fide* neutrophils purified from the *Cnr*2$^{-/-}$ spleen at day 3 after infection exhibited reduced TNF release and markedly enhanced amounts of IL-10 at a later time point as compared with WT controls (Fig. 5*E*). In accordance, higher percentages of IL-10-producing CD11b$^+$ Ly6G^{hi} neutrophils from the spleens of day 6 infected *Cnr*2$^{-/-}$

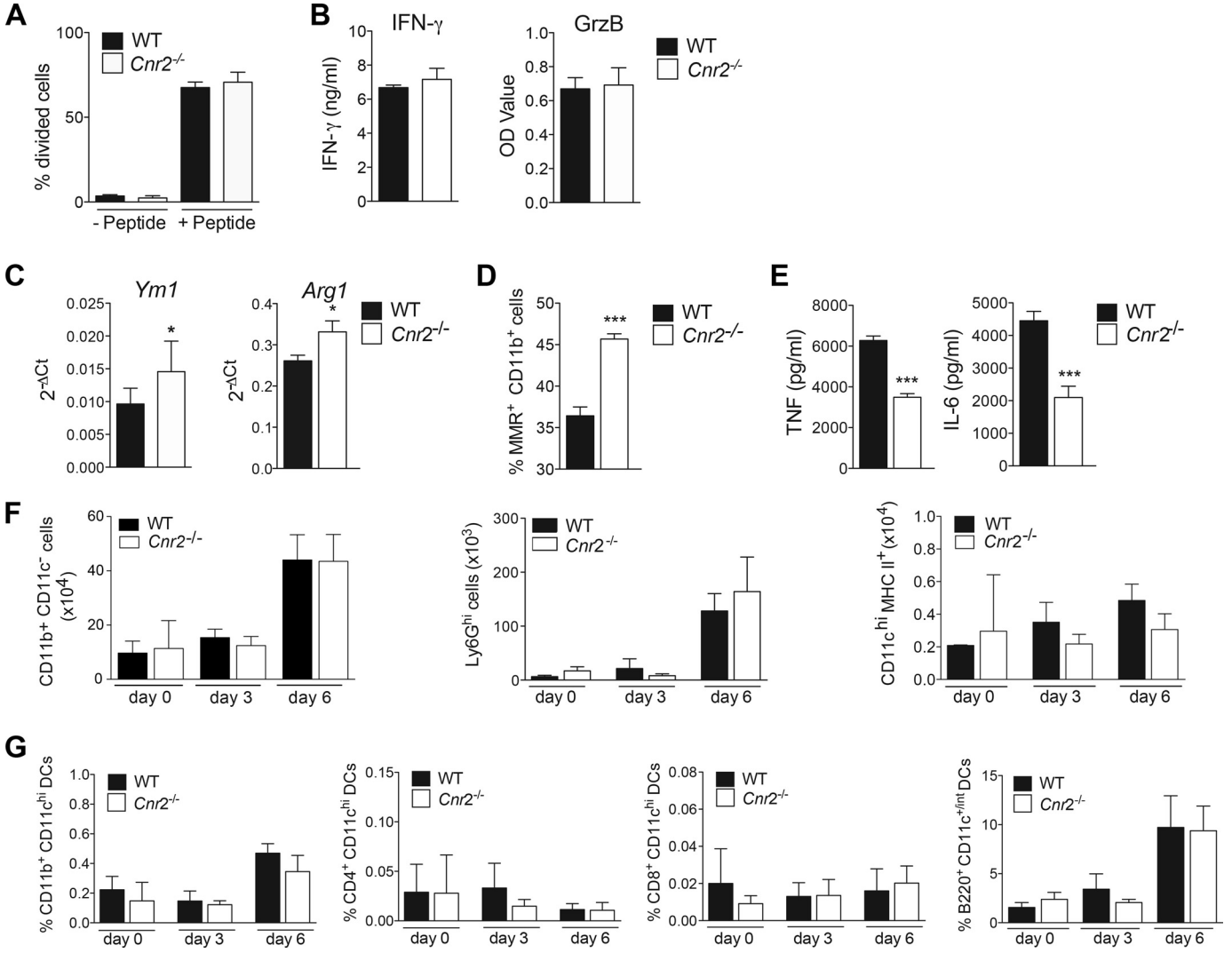

FIGURE 3. **CB2 does not affect antigen presentation capacities of BM DCs but phenotype and function of CD11b$^+$ BM macrophages.** *A*, equal T cell stimulatory capacity of WT or *Cnr2*$^{-/-}$ BM DCs. The diagram shows percentages of divided OT-II transgenic T cells after coculture with peptide-pulsed WT or *Cnr2*$^{-/-}$ BM DCs (mean ± S.E. (*error bars*), $n = 3$ mice/group). The diagram shows mean percentage ± S.E. of CFSE-positive CD4$^+$ T cells that had undergone at least one division as determined after 72 h by flow cytometry. *B*, comparable IFN-γ and GrzB production in OT-II transgenic T cells after coculture with peptide-pulsed WT or *Cnr2*$^{-/-}$ BM DCs. Shown is the amount of IFN-γ and GrzB in supernatants as determined by ELISA after 24 h of coculture (mean ± S.E., $n = 3$ mice/group). *C*, Ym1 and Arg-1 mRNA expression in WT or *Cnr2*$^{-/-}$ BM macrophages (mean ± S.E., $n = 5$–6 mice/group). *D*, enhanced percentages of MMR$^+$ CD11b$^+$ cells in LPS-stimulated *Cnr2*$^{-/-}$ BM macrophages (mean ± S.E., $n = 5$ mice/group). *E*, reduced TNF and IL-6 secretion in LPS-stimulated *Cnr2*$^{-/-}$ BM macrophages as determined by ELISA (mean ± S.E., $n = 5$–6 mice/group). *F*, numbers of CD11b$^+$ CD11c$^-$ cells, Ly6G^{hi} neutrophils, and CD11c^{hi} MHC-II$^+$ DCs in the blood of infected WT or *Cnr2*$^{-/-}$ mice. Shown are mean numbers ± S.D. (*error bars*) of cells of the indicated mice at days 0, 3, and 6 after infection ($n = 3$–4 mice/group). *G*, percentages of conventional DCs and plasmacytoid DCs in the blood of infected mice as determined by flow cytometry. Diagrams show mean percentages ± S.D. of DC subsets in the blood of the indicated mice at days 0, 3, and 6 after PbA infection. *, $p < 0.05$; ***, $p < 0.001$.

mice were detected by flow cytometry after iRBC restimulation when compared with WT control cells, whereas no differences were observed between the genotypes with regard to frequencies of TNF-producing cells (Fig. 5*F*). Proportions of TNF-producing MMMs were lower in the spleens of *Cnr2*$^{-/-}$ when compared with WT mice, whereas TNF-producing cells among the other macrophage subsets were equivalent in both mouse strains (Fig. 5*G*). All macrophage subsets in the spleens of day 6 infected *Cnr2*$^{-/-}$ mice exhibited higher percentages of IL-10-producing cells when compared with WT mice after iRBC stimulation, with the exception of CD11b$^+$ F4/80$^+$ cells (Fig. 5*G*). Taken together, these findings indicate that in the spleens of PbA-infected *Cnr2*$^{-/-}$ mice, higher frequencies as well as absolute numbers of IL-10-producing neutrophils and macrophages were present as compared with WT mice.

In the serum of WT and *Cnr2*$^{-/-}$ mice, no differences were observed in TNF and CCL2 levels during infection (Fig. 5*H*). However, reduced levels of IFN-γ, IL-1α, and IL-12 at day 3 as well as higher levels of IL-10 at day 6 hint toward reduced Th1 responses and an anti-inflammatory cytokine milieu in infected *Cnr2*$^{-/-}$ mice. These data indicate that CB2 also has an impact on systemic cytokine levels after PbA infection.

Protection against ECM in Cnr2$^{-/-}$ *Mice Depends on CCL17*—Brain infiltrates of *Cnr2*$^{-/-}$ mice contained an increased percentage of immigrating CD11b$^+$ cells that expressed MMRs$^+$ and elevated amounts of Arg-1 mRNA, whereas the fraction of MHC-II-expressing CD11b$^+$ cells was markedly reduced (Fig. 6, *A*–*C*). These cells exhibited high levels of Ly6C, indicating a monocytic origin (Fig. 6*D*). We detected no differences in the percentages of brain-infiltrating

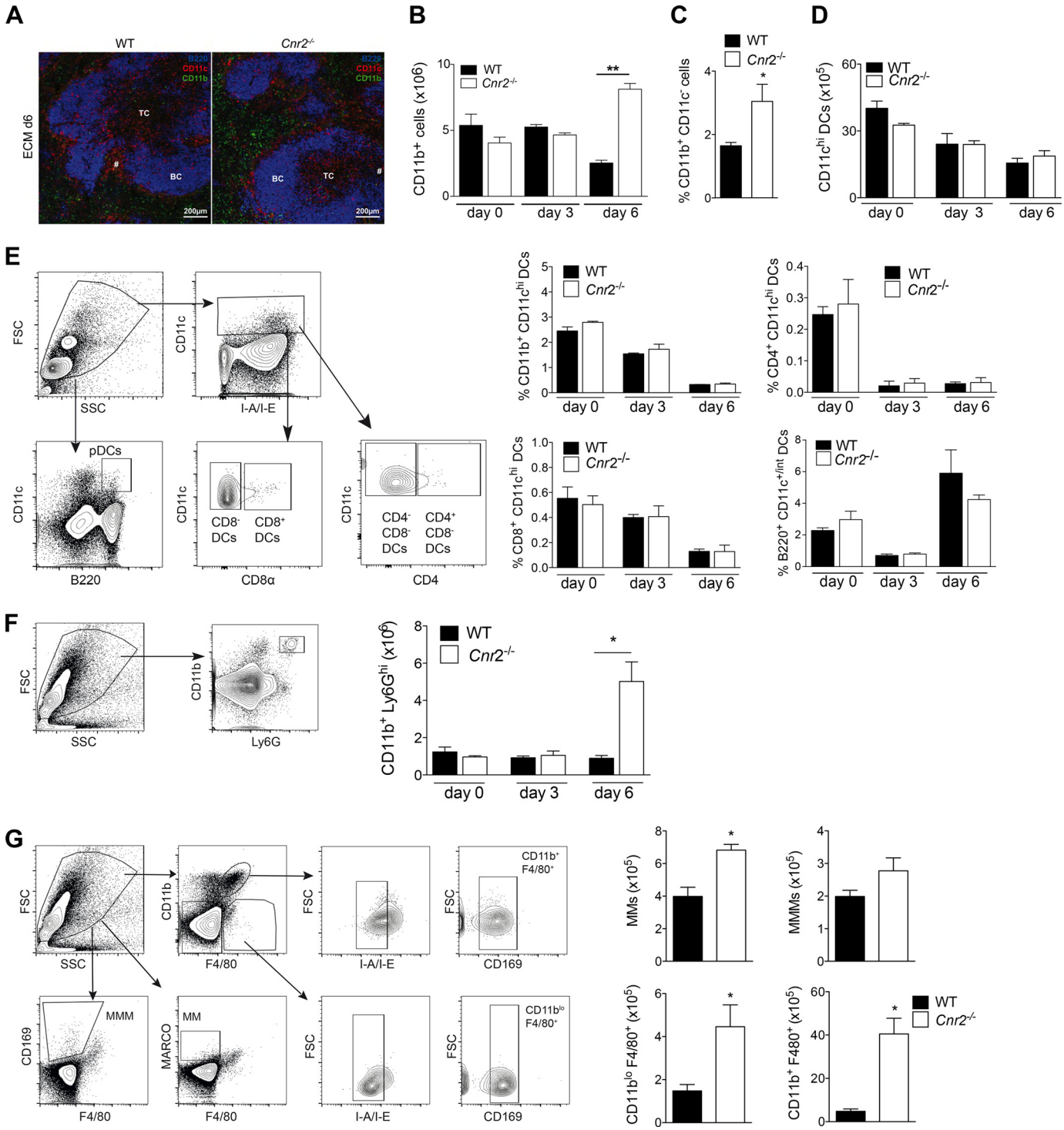

FIGURE 4. **Macrophages and neutrophils accumulate in the spleens of infected *Cnr2*$^{-/-}$ mice at day 6 when compared with WT controls.** *A*, representative spleen sections of day 6 infected WT (*left*) and *Cnr2*$^{-/-}$ (*right*) mice using immunofluorescence for B220 (*blue*), CD11c (*red*), and CD11b (*green*). *TC*, T cell zone; *BC*, B cell zone. *B*, enhanced numbers of CD11b^{+} cells in the spleens of day 6 infected *Cnr2*$^{-/-}$ mice as determined by flow cytometry (mean ± S.E. (*error bars*), $n = 8$–10 mice/group). **, $p < 0.01$. *C*, percentages of CD11b^{+} CD11c^{-} cells in the spleens of WT and *Cnr2*$^{-/-}$ mice at day 6 after PbA infection as determined by flow cytometry (mean ± S.E., $n = 4$ mice/group; *, $p < 0.05$). *D*, numbers of CD11c^{hi} DCs in the spleens of WT and *Cnr2*$^{-/-}$ mice after infection as determined by flow cytometry (mean ± S.D. (*error bars*), $n = 3$–4 mice/group). *E*, DC subsets in the spleens of WT and *Cnr2*$^{-/-}$ mice after PbA infection. Representative dot plots show gating strategies of splenic DC subsets. The diagrams show the percentages of DC subsets from the spleens of indicated mice at days 0, 3, and 6 after PbA infection (mean ± S.D., $n = 3$–4 mice/group). *F*, representative dot plot shows gating strategies for neutrophils in the spleen. The diagram shows numbers of CD11b^{+} Ly6G^{hi} cells in the spleen at days 0, 3, and 6 of WT and *Cnr2*$^{-/-}$ 6 days after PbA infection as determined by flow cytometry ($n = 3$–4 mice/group; mean ± S.E.; *, $p < 0.05$). *G*, representative dot plots showing gating strategies for macrophage subsets in the spleen. The diagram shows the numbers of macrophage subsets in the spleens of WT and *Cnr2*$^{-/-}$ at day 6 after PbA infection ($n = 4$ mice/group; mean ± S.E.; *, $p < 0.05$).

Ly6G$^+$ neutrophils or CD4$^+$ and CD8$^+$ MHC II$^+$ DCs in WT and *Cnr2*$^{-/-}$ mice (Fig. 6, *D* and *E*). No difference in MHC-II expression was observed in CD11c$^+$ DCs in WT and *Cnr2*$^{-/-}$ brains (Fig. 6*F*). Thus, in the absence of CB2, a CD11b$^+$ cell subset was recruited to the brain that expresses selected signature molecules with regulatory or recovery macrophage functions rather than effector killing functions. IFN-γ and TNF mRNA expression were also reduced, and inducible nitric-oxide synthase expression was equivalent in the brains of infected *Cnr2*$^{-/-}$ mice, underscoring a reduced local inflammatory response (Fig. 6*G*). Reduced percentages of GrzB$^+$ CD8$^+$ T cells in the brains of infected *Cnr2*$^{-/-}$ mice further indicated diminished anti-parasitic T cell responses (Fig. 6*H*). To delineate factors contributing to the protective effects of CD11b$^+$

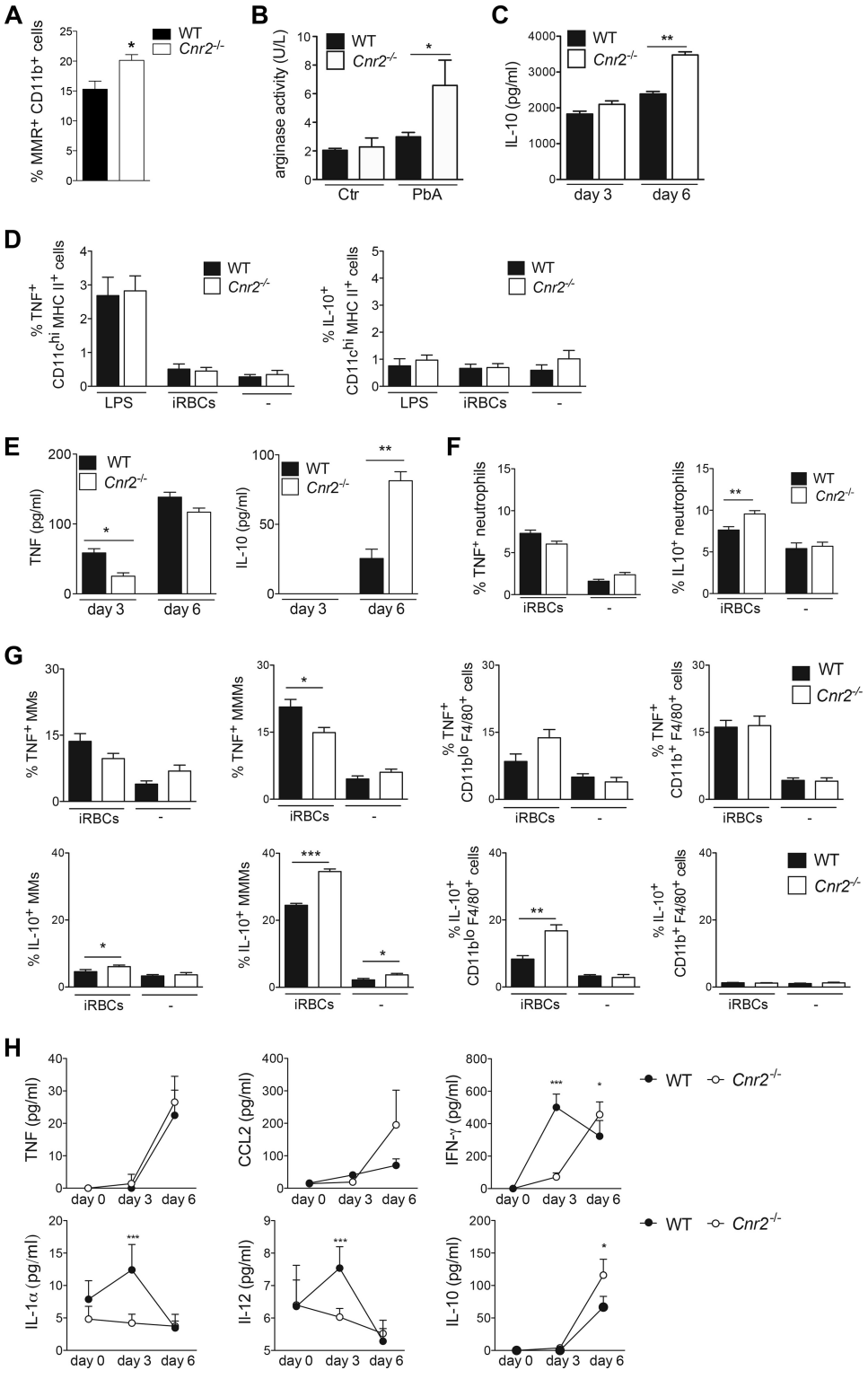

myeloid cells in *Cnr2*$^{-/-}$ mice, we focused on the CC-chemokine CCL17, because its expression is strongly enhanced in alternatively activated macrophages (32, 37) and was markedly up-regulated by IL-4 stimulation (Fig. 6*I*) (32, 38). We bred mice lacking CB2 receptors with CCL17-deficient animals (20, 39, 40) and compared the development of ECM in *Cnr2*$^{-/-}$ mice that also lacked CCL17 on one (*Cnr2*$^{-/-}$/*CCL17*$^{+/-}$) or both alleles (*Cnr2*$^{-/-}$/*CCL17*$^{-/-}$). *Cnr2*$^{-/-}$/*CCL17*$^{+/-}$ mice were protected against ECM, as shown before. In sharp contrast, PbA-infected *Cnr2*$^{-/-}$/*CCL17*$^{-/-}$ animals were no longer protected against ECM (Fig. 6*J*). In addition, the clinical score was reduced in *Cnr2*$^{-/-}$/*CCL17*$^{+/-}$ animals when compared with *Cnr2*$^{-/-}$/*CCL17*$^{-/-}$ mice (Fig. 6*K*). These data show that CCL17 is an essential mediator for the protective effects of CB2 deletion.

Discussion

In this study, we demonstrate a role of CB2 in the pathophysiology of experimental CM. *Cnr2*$^{-/-}$ mice exhibit enhanced survival, a reduced parasite load in the brain, and a diminished BBB disruption after PbA infection in comparison with WT mice. Importantly, we demonstrate that therapeutic application of a CB2 antagonist conferred increased CM resistance in C57BL/6 mice. These results indicate a therapeutic potential of targeting CB2 signaling in ECM and may also facilitate the design of human intervention trials for the treatment of parasite-induced encephalitis.

It was suggested that CB2 could act as a chemokine receptor and is therefore functionally involved in immune cell trafficking (41–44). Here we showed that CB2 controls the recruitment of peripheral immune cells into the brain during ECM. The degree of mononuclear cells infiltrating the brain was markedly reduced in PbA-infected *Cnr2*$^{-/-}$ mice. The most striking finding was the nature of the immune cells invading the brain in these animals. Brain infiltrates in infected *Cnr2*$^{-/-}$ mice showed reduced numbers of lymphoid CD8$^+$ T cells. In contrast, we found that CD11b$^+$ cells markedly expanded in the spleen, and higher proportions of these cells were determined in brain infiltrates of infected *Cnr2*$^{-/-}$ mice.

Our findings suggest that increased numbers of CD11b$^+$ cells in *Cnr2*$^{-/-}$ *versus* WT spleens represent myeloid macrophages as well as neutrophils. Among those, the specific subset of CD11b$^+$ F4/80^{hi} CD169^{lo} MHC-II^{lo} cells increased in the spleens of infected *Cnr2*$^{-/-}$ animals. A corresponding population of F4/80$^+$ CD11b$^+$ cells has recently been described as a macrophage subset that accumulated after IL-33 treatment in the spleens of PbA-infected C57BL/6 mice and mediated resistance to CM due to anti-inflammatory properties (45). However, CD11b has also been described on subsets of adaptive immune cells among those CD8$^+$ T cells (46). Although our findings exclude a differential increase of the major adaptive immune cell subsets in infected *Cnr2*$^{-/-}$ mice, we cannot fully exclude the possibility that minor populations of non-myeloid CD11b-expressing cells also accumulate in the *Cnr2*$^{-/-}$ spleen.

We identified CB2-expressing myeloid cells as a critical cell type contributing to enhanced susceptibility to ECM in mixed BM chimeras. It is well established that myeloid-derived macrophages express pattern recognition receptors and phagocytose blood pathogens for subsequent transfer to local DCs for cross-presentation to specific T cells (47). Alternatively activated macrophages are specialized in down-regulating immune responses by a specific anti-inflammatory response pattern (32). *In vitro*, we found a polarization of *Cnr2*$^{-/-}$ BM macrophages toward M2. In the spleens of infected *Cnr2*$^{-/-}$ mice, expanded CD11b$^+$ cells expressed higher levels of selected M2 markers, such as CD206 (macrophage mannose receptor), arginase-1 activity, and IL-10, an anti-inflammatory cytokine known to confer protection against ECM (48, 49). Macrophage subsets and neutrophils expanded in the spleens of *Cnr2*$^{-/-}$ mice after infection and further exhibited an enhanced capacity to produce IL-10. Also, in the brains of infected *Cnr2*$^{-/-}$ mice, immigrating CD11b$^+$ cells expressed higher CD206 and reduced MHC-II levels, associated with enhanced arginase-1 production. Furthermore, expression of M1-associated cytokines was reduced in the *Cnr2*$^{-/-}$ brain when compared with WT. In contrast, we found a concomitant and equivalent expression of the M1-associated cytokine TNF in the majority of splenic macrophages in both genotypes. Thus, rather then representing canonical M2 macrophages, expanded CD11b$^+$ cells in infected *Cnr2*$^{-/-}$ mice share only selected factors with anti-inflammatory myeloid cells after PbA infection. In fact, multiple reports defined CD11b$^+$ cells as a highly heterogeneous mixture of cells that also include a subset of myeloid-derived suppressor cells (MDSCs) (50). MDSCs have been shown to stain positive for Gr-1, an antibody detecting both Ly6C and Ly6G. A major subset of CD11b$^+$ cells in infected *Cnr2*$^{-/-}$ mice also expressed Ly6C^{hi} and Ly6G^{hi} surface molecules, thus reflecting the phenotype of certain MDSC subsets phenotypically identical to neutrophils or inflammatory monocytes (50). MDSCs exhibit potent immunosuppressive activity on T cell functions *ex vivo* via mechanisms that depend on nitric oxide, arginase, IFN-γ, and cell-cell contact and have functionally

FIGURE 5. **Enhanced expression of MMR, arginase-1 activity, and IL-10 in CD11b$^+$ cells and higher IL-10 production by macrophages and neutrophils in the spleens of infected *Cnr2*$^{-/-}$ mice.** *A*, percentages of MMR$^+$ CD11b$^+$ cells in the spleens of day 6 infected WT and *Cnr2*$^{-/-}$ mice as determined by flow cytometry (mean ± S.E. (*error bars*), $n = 5$–6 mice/group). *B*, measurement of functional arginase-1 activity in spleen-isolated CD11b$^+$ cells of control or day 6 infected mice. One representative experiment of two independent experiments is shown in each section (mean ± S.E., $n = 5$–10 mice/group). *C*, IL-10 secretion in spleen-isolated CD11b$^+$ cells from WT and *Cnr2*$^{-/-}$ mice at day 3 and day 6 after PbA infection after rechallenge with LPS for 15 h (mean ± S.E., $n = 5$–6 mice/group). *D*, diagrams show mean percentages of cytokine-secreting CD11c^{hi} MHC II$^+$ DCs from the spleens of WT and *Cnr2*$^{-/-}$ mice 15 h after stimulation with iRBCs or unstimulated as determined by flow cytometry (mean ± S.E., $n = 4$ mice/group). *E*, TNF and IL-10 production by MACS-purified Ly6G$^+$ neutrophils isolated from the spleens of WT and *Cnr2*$^{-/-}$ mice at day 3 or 6 after PbA infection as determined after rechallenge with LPS for 15 h by cytokine bead assays (mean ± S.E., $n = 3$–5 mice/group). *F*, diagrams show percentages of cytokine-secreting Ly6G^{hi} neutrophils from the spleens of day 6 infected *Cnr2*$^{-/-}$ and WT mice 15 h after stimulation with iRBCs or unstimulated as determined by flow cytometry (mean ± S.E., $n = 4$ mice/group). *G*, diagrams show mean percentages of cytokine-secreting macrophage subsets from day 6 infected WT and *Cnr2*$^{-/-}$ mice 15 h after stimulation with iRBCs or unstimulated as determined by flow cytometry (mean ± S.E., $n = 4$ mice/group). *H*, cytokine concentrations in the blood from WT and *Cnr2*$^{-/-}$ mice at days 0, 3, and 6 after PbA infection as determined by cytokine bead assays (mean ± S.E., $n = 3$–5 mice/group). *, $p < 0.05$; **, $p < 0.01$; ***, $p < 0.001$.

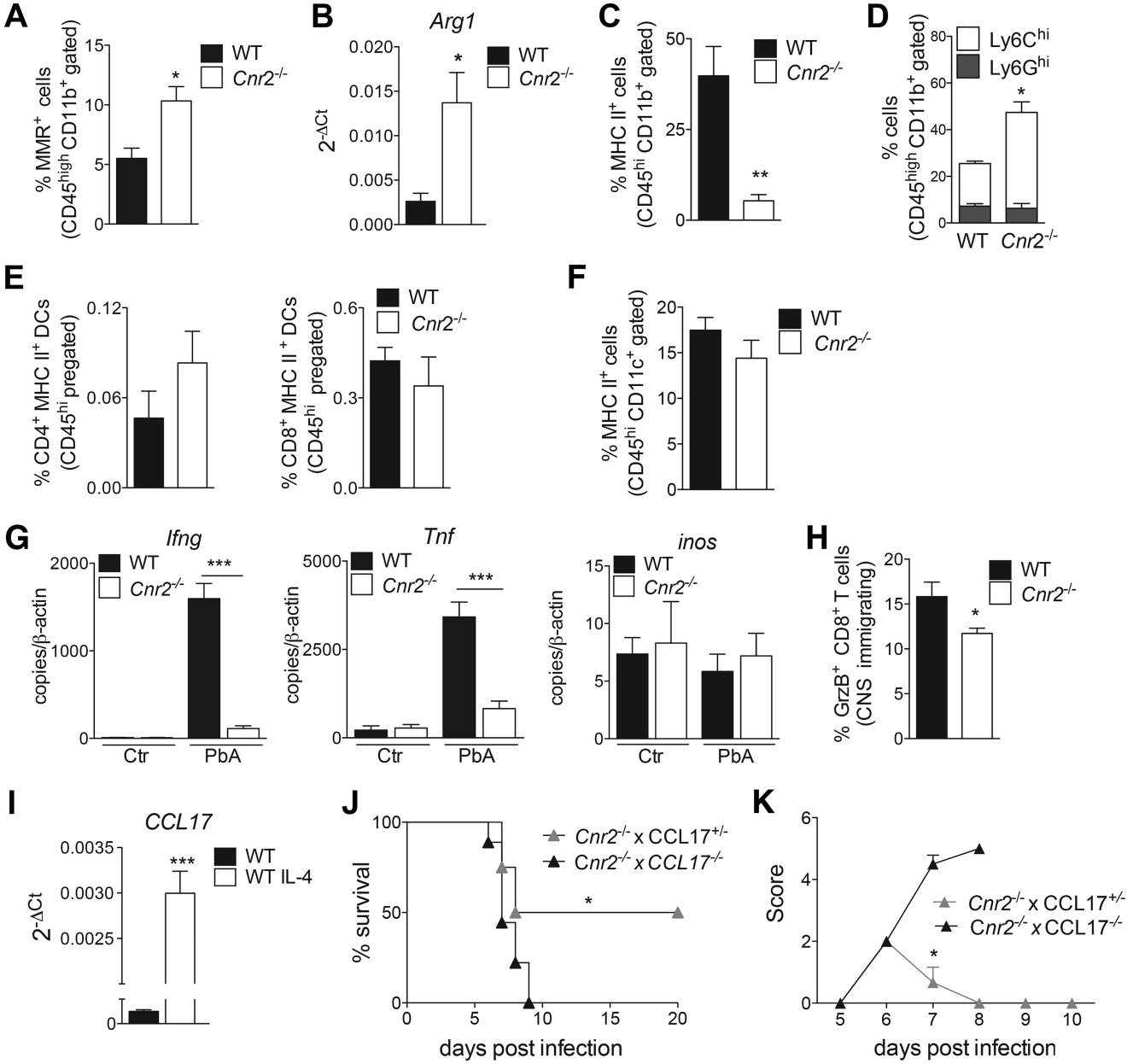

FIGURE 6. **CCL17 mediates protection against ECM in *Cnr2*$^{-/-}$ mice.** *A*, percentages of MMR^{+} brain-infiltrating cells (pregated for CD45^{hi} and CD11b expression) in WT and *Cnr2*$^{-/-}$ mice at day 6 after PbA infection as determined by flow cytometry (mean ± S.E. (*error bars*), $n = 4$ mice/group). *B*, Arg-1 mRNA expression in mononuclear cells isolated from the brains of WT and *Cnr2*$^{-/-}$ mice at day 6 after PbA infection. mRNA levels are normalized to GAPDH expression (mean ± S.E., $n = 4$ mice/group). *C*, percentages of MHC-II^{+} CD45^{hi} CD11b^{+} brain-infiltrating cells in WT and *Cnr2*$^{-/-}$ mice at day 6 after PbA infection (mean ± S.E., $n = 5$–7 mice/group). *D*, percentages of Ly6C^{hi} (*open bars*) and Ly6G^{hi} (*filled bars*) brain-infiltrating cells (pregated for CD45^{hi} and CD11b expression) in WT and Cnr2$^{-/-}$ mice at day 6 after PbA infection as determined by flow cytometry (mean ± S.E., $n = 4$–5 mice/group). *E*, percentages of CD4^{+} CD11c^{+} DCs and CD8^{+} CD11c^{+} DCs (pregated for CD45^{hi} MHC II^{hi} cells) immigrating into the brains of day 6 infected WT and *Cnr2*$^{-/-}$ mice as determined by flow cytometry (mean ± S.E., $n = 4$ mice/group). *F*, percentages of MHC-II^{+} CD45^{hi} CD11c^{+} brain-infiltrating cells in WT and *Cnr2*$^{-/-}$ mice at day 6 after PbA infection (mean ± S.E., $n = 4$ mice/group). *G*, *Ifng*, *Tnf*, and *inos* mRNA expression in the brains of control or day 6 PbA-infected WT or *Cnr2*$^{-/-}$ mice. mRNA levels are normalized to *β*-actin expression, and results are presented as the mean ± S.E. ($n = 3$–5 mice/group). *H*, percentages of GrzB^{+} CD8^{+} TCR^{+} T cells infiltrating into the brains of WT or *Cnr2*$^{-/-}$ mice at day 6 after infection with 5×10^4 PbTg OVA. The diagram shows percentages of cells (pregated for CD45^{hi} expression) (mean ± S.E., $n = 6$ mice/group). *I*, CCL17 mRNA expression in M2 polarized BM macrophages from C57BL/6 mice after differentiation with M-CSF and IL-4 (mean ± S.E., $n =$ 5–6 mice/group). *J*, survival of *Cnr2*$^{-/-} \times$ CCL17$^{+/-}$ and *Cnr2*$^{-/-} \times$ CCL17$^{-/-}$ mice after PbA infection. One representative experiment of two independent experiments is shown ($n = 5$–10 mice/group). *K*, clinical score of PbA-infected *Cnr2*$^{-/-} \times$ CCL17$^{+/-}$ and *Cnr2*$^{-/-} \times$ CCL17$^{-/-}$ mice ($n = 10$–12 mice/group). *, $p < 0.05$; **, $p < 0.01$; ***, $p < 0.001$.

been involved in parasitic infections (51, 52). Previous studies demonstrated that CB1 as well as CB2 are involved in the induction of MDSC in mice following THC treatment (53). We found that CD11b^{+} cells in infected *Cnr2*$^{-/-}$ mice shared markers with MDSC, such as low levels of MHC class II and enhanced arginase-1 activity. Future studies will precisely define the origin and function of expanded CD11b^{+} cells in infected *Cnr2*$^{-/-}$ mice.

We further determined that splenic *Cnr2*$^{-/-}$ neutrophils markedly increased in the spleens of infected *Cnr2*$^{-/-}$ mice and shifted toward an anti-inflammatory cytokine profile. Also, in the blood, reduced Th1 responses and a bias toward anti-in-

flammatory cytokines were detected in infected *Cnr2*$^{-/-}$ mice. These findings were unexpected, because earlier data indicated that CB2 activation inhibited alternative but also classical marker expression in brain-derived microglia/macrophages in an ischemic stroke model or even favored IL-10 production in LPS/IFN-γ stimulated murine peritoneal macrophage and the transition to an M2 phenotype in liver macrophages (Kupffer cells) (22, 54, 55). These data, in comparison with our findings, may reflect cell-specific differences of CB2 functions that depend on culture conditions, the characteristics of the pathogen, or the respective CB2-expressing myeloid cell subset *in vivo*.

Parasite-specific cytotoxic T cells in the spleen induced by antigen-presenting cells are critical mediators of ECM-associated pathology (8, 56–63). We demonstrate that anti-parasitic T cell responses were reduced in the brains and spleens of infected *Cnr2*$^{-/-}$ mice. We also identified a reduced vascular leakage in the brains of infected *Cnr2*$^{-/-}$ mice. It is possible that the maintenance of the BBB in *Cnr2*$^{-/-}$ mice is related to the observed reduction in brain-immigrating CD8$^+$ T lymphocytes, which have been implicated as cellular mediators of BBB breakdown via perforin-dependent mechanisms (61, 62). However, production of cytolytic factors was only reduced in whole spleen cultures but not in isolated splenic CD8 T lymphocytes of infected *Cnr2*$^{-/-}$ mice. This suggests that suppressive effects in the *Cnr2*$^{-/-}$ spleens affected anti-parasitic T cell responses required for ECM induction but did not operate in a T cell intrinsic way. Generation of mixed BM chimeras further demonstrated that the expression of CB2 on myeloid cells was associated with mortality after PbA infection. Corroborating our *in vivo* data, we found comparable GrzB and IFN-γ production by *Cnr2*$^{-/-}$ and WT CD8$^+$ T cells upon stimulation by peptide-loaded CB2-expressing RAG-2$^{-/-}$ DCs *in vitro*, indicating that CB2 modulates myeloid responses but does not directly affect T cell functions under these conditions. Nevertheless, we cannot fully exclude the possibility that CD8$^+$ T cells contributed to enhanced protection in PbA-infected *Cnr2*$^{-/-}$ mice by using alternative effector functions, such as perforin.

The M2 macrophage chemokine CCL17 is an essential factor that mediates enhanced protection against ECM in the absence of CB2 as demonstrated by the full susceptibility of CCL17 × *Cnr2* double-deficient mice to ECM. We demonstrated before that the CCL17/CCR4 axis affects the function of CCR4$^+$ myeloid cells, but not T lymphocytes, recruited into the brain during CNS autoimmunity (64). It is thus possible that CCL17 favors brain recruitment or function of myeloid cells rather than CD8$^+$ T cells in ECM with beneficial outcome in disease in *Cnr2*$^{-/-}$ mice. Here we propose a model whereby CB2 is critical for the development of potent anti-parasitic immune responses early during PbA infection *in vivo*, thereby causing disease pathology. Pharmacological intervention with a CB2 antagonist induced enhanced disease protection, pointing toward its potential for the treatment of fatal malaria in humans. Clinical studies will help to move toward the development of applications using antagonists/inverse agonists acting on CB2 receptors in fatal malaria.

Experimental Procedures

Mice—C57BL/6 (H-2^b) and RAG-2 knock-out female mice were purchased from Janvier (France) and/or bred locally. CB2-deficient (*Cnr2*$^{-/-}$, N10 backcross to C57BL/6) and CCL17$^{-/-}$ mice (39) and wild type mice were bred locally. All animals were bred and housed according to German guidelines for animal care and the European Union animal welfare guidelines. Ethical approval for the use of all mice in this study was obtained from the Landesamt für Natur, Umwelt und Verbraucherschutz (LANUV), Cologne, Germany (AZ 8.87–50.10.31.08.271).

Endocannabinoid Measurements—Brain endocannabinoid and arachidonic acid levels were measured by GC/MS as reported previously (65). In short, immediately frozen brains were cut along their longitudinal axis and weighed. Chloroform was added (1 ml/100 mg), and the half-brains were homogenized with a Polytron homogenizer (15,000 rpm for 1 min) and sonicated twice for 10 s. The homogenate was added to 10 ml of ice-cold chloroform containing the internal standards (328 pmol of AA-d_8, 529 pmol of 2-AG-d_5). Folch extraction was performed by adding 5 ml of methanol and 2.5 ml of PBS. The mixture was vigorously vortexed and sonicated for 5 min at 4 °C, followed by centrifugation for 5 min at 800 × *g*. The organic phase was recovered into a glass vial and dried under N_2. The dried organic phase was reconstituted into 1 ml of EtOH and vortexed, and 9 ml of water were added. Solid phase extraction was performed with Sep-Pak cartridges (Waters). Columns were conditioned with 3 ml of methanol (99.8%) and 3 ml of 10% ethanol, and then the samples were applied and washed with 3 ml of 10% ethanol. The arachidonic acid and 2-AG were eluted with 3 ml of ethyl acetate/acetonitrile (8:2). Eluates were dried under N_2 and reconstituted in 50 μl of acetonitrile. 20 μl of *N*,*N*-diisopropylethylamine (Sigma) and 20 μl of pentafluorobenzyl bromide (Sigma) (1 g in 3 ml of acetonitrile) were added and incubated for 25 min at 45 °C to derivatize arachidonic acid. Excess reagent was evaporated, the sample was reconstituted in 25 μl of dimethylisopropylsilylimidazole (TCI Europe), and 2-AG was derivatized with it for 1 h at room temperature. Samples were stored at −20 °C until GC/MS analysis. Samples were injected in splitless mode into an Agilent 6890N GC (HP-5MS column, 30 m). The oven temperature program was as follows: initial temperature 150 °C for 1 min, followed by an 8 °C/min increase up to 280 °C, which was held for 10 min. Helium was used as a carrier gas at a flow rate of 1.5 ml/min. Coupled to the GC was an Agilent 5975C MSD system. The following ions were used for selected ion monitoring analysis: 2-AG/1-AG, *m*/*z* 535; 2-AG-d_5/1-AG-d_5, *m*/*z* 540; AA, *m*/*z* 386, 484; AA-d_8, *m*/*z* 392. Because of a significant amount of spontaneous acyl group migration (isomerization) of 2-AG during extraction, the peak areas of 1(3)-AG and 2-AG were combined for quantitative analysis.

Infection, Treatment, and Vascular Leakage—PbA or OVA-expressing *P. berghei* (PbTg) parasitized red blood cells (RBCs) (kindly provided by Rachel Lundie and Andrew Waters) were used (59). 8–12-week-old mice were infected intravenously with 5 × 10^4 PbA-RBCs obtained from donor mice infected intraperitoneally with 1 × 10^7 PbA-RBCs. Parasitemia was

assessed daily after day 4 in Giemsa-stained tail blood smears. The course of disease was monitored twice daily using the following score according to Amante *et al.* (27): 0, without symptoms; 1, ruffled fur; 2, hunching; 3, wobbly gait; 4, limb paralysis; 5, convulsions; 6, coma. Each sign was given a score of 1. Animals with severe ECM (cumulative score of 5) and severe anemia were sacrificed according to ethics guidelines. For pharmacological treatment, C57BL/6 mice were daily intraperitoneally injected with 25 μg of CB2 antagonist SR144528 (RTI International) in DMSO and PBS. Control groups were injected with DMSO and PBS. The dose of SR144528 was chosen in accordance with earlier studies (66–68). For assessment of vascular leakage, mice were intravenously injected with 200 μl of 2% Evans Blue (Sigma-Aldrich) at day 6 post-infection, and 1 h later, brains were analyzed for dye leakage. After photodocumentation, brains were weighed and incubated in 2 ml of formamide for 48 h at 37 °C. 100 μl of solution were analyzed in triplicate. Absorbance was measured at 620 nm in an ELISA reader. Concentration of Evans Blue was calculated with a standard curve starting at 200 μg/ml and is expressed as μg of Evans Blue/g of brain tissue.

Isolation of Mouse Parasites—Preparation of iRBCs was performed based on earlier published protocols (36). In brief, blood from PbA-infected mice was diluted with PBS (pH 7.4) and centrifuged on Lymphoprep cushions at room temperature for 15 min. After removal of the buffy coat, cell pellets were resuspended in PBS before usage.

Generation of BM Chimeric Mice—Recipient mice were irradiated with 9.5 Grays and reconstituted with $0.8–1.2 \times 10^7$ BM cells (or $0.4–0.6 \times 10^7$ cells mixed with $0.4–0.6 \times 10^7$ BM cells from the indicated donors in mixed chimeras) via tail vein injection ~7–8 h after irradiation. Mice were treated with antibiotics (trimethoprim and sulfamethoxazole) for 9 days after reconstitution. The level of chimerism was determined by assessing the percentage of CD45.2 donor cells present in the blood of CD45.1 recipients by flow cytometry 7–8 weeks after BM cell transfer. Mice exhibiting >95% $CD45.2^+$ donor cells in peripheral blood cells were PbA-infected as described above.

Cell Isolation—Brain tissue samples were collected from perfused animals, homogenized by digestion with collagenase/dispase (Roche Applied Science) and DNase I (Roche Applied Science, Mannheim, Germany) at 37 °C for 45 min, and gently pressed through a sieve to obtain single cell suspensions. For enrichment of brain mononuclear cells, 30 and 70% Percoll gradients (GE Healthcare UK Ltd., Buckinghamshire, England) were performed and centrifuged at $922 \times g$ for 25 min without brake at room temperature. Cells within the interphase were collected. Splenocytes were isolated by digestion with collagenase type VIII and DNase I (Sigma-Aldrich). $CD11b^+$ cells from spleens were purified in two steps. First, $CD11c^+$ cells were purified from spleens via bead-coupled antibodies (CD11c MicroBeads, Miltenyi Biotec, Bergisch Gladbach, Germany), and the flow-through was subsequently purified for $CD11b^+$ cells (CD11b MicroBeads, Miltenyi Biotec). To isolate splenic neutrophils, the Anti-Ly-6G MicroBead Kit (Miltenyi Biotec) was used. Purified cell populations were cultured in 1×10^6 cells/ml in DMEM supplemented with 10% (v/v) heat-inactivated FCS, 1% MEM, 1% penicillin-streptomycin, 0.1% 2-mercaptoethanol (all from Gibco) and stimulated with 100 ng/ml *Escherichia coli* LPS serotype 0127:B8 (Sigma-Aldrich) for 16 h. For isolation of lymphoid cells, spleens were gently pressed through a sieve to obtain single lymphocyte suspensions. Lymphocyte isolation from the blood of mice was performed by pipetting freshly drawn blood into ice-cold PBS containing 5 mM EDTA (150 μl of blood, 2 ml of PBS-EDTA). Samples were inverted immediately to prevent clotting. Red blood cells were digested using ACK lysing buffer (Gibco) as described by the manufacturer. Erythrocytes from the blood were isolated via Pancoll gradient isolation (Pan-Biotech) with centrifugation at 1400 rpm/room temperature without brake for 20 min.

Coculture and Proliferation Assays—1×10^5 BM DCs were incubated for 3 h at 37 °C, 5% CO_2 in a 100-μl total volume of BM DC medium with or without 1 μM I-Ab OVA(323–339) peptide. Splenocytes were incubated with CFSE (1 μM in PBS) for 20 min at 37 °C in the dark. 1×10^5 CFSE-labeled $CD4^+$ OT-II cells were cocultured with peptide-pulsed or control BM DCs for 3 days. Proliferation was determined on day 3 via flow cytometry.

Flow Cytometry—After FC receptor blockade with anti-CD16/32 mAb (Biozol, Eching, Germany), cells were stained with phycoerythrin-, allophycocyanin-, Alexa Fluor 488-, Alexa Fluor 647-, BV421-, BV510-, or biotin-conjugated mAbs in combination with cyanine 5.5/streptavidin/peridininchlorophyll. mAbs against TCR β-chain, CD4, CD8α, CD45, CD40, CD80, CD86, I-A/I-E, CD11b, CD11c, GrzB, Ly6C, Ly6G, Nk1.1, B220, CD169, F4/80, TNF, and IL-10 (eBiosciences or Biolegend (San Diego, CA)) and MARCO (ABD Serotec) were used. Intracellular TNF and IL-10 staining was performed according to the manufacturer's protocol (Biolegend). Intracellular FoxP3 staining with the anti-mouse/rat FoxP3 staining kit was performed according to the manufacturer's protocol (eBiosciences). Acquisition and analysis were performed with FACSCanto (BD Biosciences) and FlowJo™ software (Tree Star, Ashland, OR).

Generation and in Vitro Stimulation of BM Macrophages and Dendritic Cells—BM cells for generation of BM DCs were isolated from the hind legs of mice, and 5×10^5 cells/ml were cultured in DMEM supplemented with 10% (v/v) heat-inactivated FCS, L-glutamine, MEM, penicillin/streptomycin, 2-mercaptoethanol (all from Gibco), and 10% GM-CSF, and medium was changed at day 3 of culture. BM cells for generation of macrophages were cultured in 1.5×10^5 cells/ml in RPMI supplemented with 10% (v/v) heat-inactivated FCS, L-glutamine, MEM, penicillin/streptomycin, 2-mercaptoethanol (all from Gibco), and 15% conditioned medium of L292 cells. On day 3, adherent cells were recultured in complete medium and harvested on day 6. BM-derived macrophages were stimulated *in vitro* for the indicated times with 100 ng/ml *E. coli* LPS serotype 0127:B8 (Sigma-Aldrich). For the generation of M2 macrophages, M-CSF-differentiated BM macrophages from WT and $Cnr2^{-/-}$ mice were stimulated with IL-4 at a concentration of 100 units/ml for 48 h (eBiosciences; biological activity 8×10^5 units/mg). After stimulation, cells were used for flow cytometry or frozen in TRIzol for further quantitative real-time PCR analyses. BM macrophage cells or the indicated splenic cells were

stimulated on day 5 or 6, respectively, for 15 h with 5×10^4 iRBCs/well.

Measurement of Cytokines—Cytokines in culture supernatants were determined by a specific sandwich enzyme-linked immunosorbent assay. TNF, IL-6, IFN-γ, IL-10, and GrzB (ELISA Duo-Set, R&D Systems) were used according to the manufacturer's instructions. Plates were read at 450 nm using a SpectraMax 340 microtiter reader (Molecular Devices, Sunnyvale, CA). To determine cytokine levels in the serum or supernatants of $CD11b^+$ and $Ly6G^+$ splenocytes, the LEGENDplex™ multi-analyte flow assay kits (Biolegend) were used according to the manufacturer's recommendations. Serum samples were diluted 2-fold with assay buffer, whereas cell culture supernatants were assayed without dilution. Data analysis was performed using the LEGENDplex™ data analysis software (Biolegend).

Serum Preparation—To collect serum samples, blood was drawn and transferred into clotting activator containing 1.3-ml microtubes (Sarstedt, Nuembrecht, Germany). Coagulation occurred for 30 min at room temperature.

Measurement of Arginase Activity—Splenocytes were prepared as described above. The homogenate was purified for $CD11b^+$ cells via bead-coupled antibodies (CD11b MicroBeads, human and mouse, Miltenyi Biotec) using the autoMACS Pro Separator (Miltenyi Biotec). The measurement of arginase from supernatant of lysed cells was performed according to the manufacturer's protocol (Arginase Assay Kit, Abnova, Jhongli, Taiwan).

Immunofluorescence—For histological analysis, brain tissues were fixed in 4% buffered formalin and embedded in paraffin. Tissue was then sliced (4–6 μm) and stained with hematoxylin. Spleens were fixed in 4% paraformaldehyde at 4 °C for 30–120 min, washed twice in PBS, saturated in 20% sucrose for 8 h, embedded in tissue-freezing medium (Leica), and snap-frozen in 2-methylbutane (Merck) prechilled with liquid nitrogen. Samples were then sliced into 10–12-μm slices, fixed in acetone (Merck), and stained with biotinylated monoclonal rat anti-mouse Abs for CD11b, CD11c, B220, TCR, CD4, and CD8 (all purchased from eBiosciences). Bound antibody was detected using Streptavidin Alexa 647 (eBiosciences), and samples were mounted with Fluoromount-G (Southern Biotechnology Associates, Inc.) for imaging with confocal microscopy. Adobe Photoshop was used for final image processing.

Total RNA Preparation and Taqman Analysis—Mouse tissue or cells were rapidly dissected, snap-frozen in isopentane, and stored at −80 °C. Total RNA was prepared according to the TRIzol method (Invitrogen). Up to 5 μg of RNA and 0.5 μg of oligo$(dT)_{20}$ primer (Invitrogen) were heated at 70 °C for 4 min, chilled on ice, and then reverse transcribed at 42 °C for 50 min. A total volume of 20 μl included 4 μl of first strand buffer (Invitrogen), 2 μl of 0.1 M DTT, 1 μl of 10 mM dNTPs, 0.5 μl of RNase OUT (Invitrogen), and 200 units of Superscript II reverse transcriptase (Invitrogen). Quantitative RT-PCR of cDNA samples was performed using an ABI 7900 sequence detector (PerkinElmer Life Sciences) and Universal PCR Master Mix (PerkinElmer Life Sciences). After incubation of the samples at 50 °C for 2 min and 95 °C for 10 min, 40 cycles of 95 °C for 15 s and 60 °C for 1 min were applied. Taqman primer and probe sets were ordered from Applied Biosystems as follows: Cnr1 Mm01212171_s1, Cnr2 Mm00438286_m1, diacylglycerol lipase α Mm00813830_m1, diacylglycerol lipase β Mm00523381_m1, fatty acid amide hydrolase Mm00515684_m1, monoacylglycerol lipase Mm00449274_m1, ARG Mm00475988_m1. Results are expressed as -fold change relative to the control samples normalized to GAPDH. RT-PCRs for *Ifng*, *Tnf*, and *inos* were performed as described before (69). RT-PCR was performed in accordance for YM1 (ym-1 primer, gcccttattgagaggagcttta (forward) and tacagcagacaagacatcc (reverse); plasmodial 18S RNA, ctaacatggctttgacgggta (forward) and tgtcactaccctcttattt (reverse)).

Statistical Analysis—Analysis of variance and Bonferroni post hoc tests or two-tailed Student's *t* tests were used to determine differences between groups unless stated otherwise. Mann-Whitney *U* tests were used as indicated. Data are given as mean ± S.E. The Mantel-Cox log-rank test was used to compare differences in survival and clinical score between groups. All tests were performed with GraphPad Prism version 5 (GraphPad Software, San Diego, CA). $p \leq 0.05$ was considered significant, and asterisks indicate significance: *, $p < 0.05$; **, $p < 0.01$; ***, $p < 0.001$.

Author Contributions—J. A., S. Specht, W. M., S. Scheu, A. H., and A. Z. conceived and coordinated the study. J. A., S. Scheu, H. A., B. S., K. S., C. R., R. L., A. K., A. D., J. M. K., K. P., M. F., Ö. A., and D.-M. O. performed the experiments and analyzed the data; J. M. and J. G. performed endocannabinoid measurements. J. A., S. Specht, J. G., I. F., S. Scheu, A. H., and A. Z. wrote the paper. All authors read and approved the manuscript.

Acknowledgments—We thank A. Wojtalla for support with mouse breeding; A. Fattahi-Mehr, Ö. Yilmaz, B. Dubben, Patricia Jebett Korir, and A.-L. Leumann for excellent technical assistance; and M. Hübner and A. Limmer for critical discussion.

References

1. Hunt, N. H., Golenser, J., Chan-Ling, T., Parekh, S., Rae, C., Potter, S., Medana, I. M., Miu, J., and Ball, H. J. (2006) Immunopathogenesis of cerebral malaria. *Int. J. Parasitol.* **36,** 569–582
2. Belnoue, E., Potter, S. M., Rosa, D. S., Mauduit, M., Grüner, A. C., Kayibanda, M., Mitchell, A. J., Hunt, N. H., and Rénia, L. (2008) Control of pathogenic $CD8^+$ T cell migration to the brain by IFN-γ during experimental cerebral malaria. *Parasite Immunol.* **30,** 544–553
3. Snow, R. W., Guerra, C. A., Noor, A. M., Myint, H. Y., and Hay, S. I. (2005) The global distribution of clinical episodes of *Plasmodium falciparum* malaria. *Nature* **434,** 214–217
4. de Souza, J. B., Hafalla, J. C., Riley, E. M., and Couper, K. N. (2010) Cerebral malaria: why experimental murine models are required to understand the pathogenesis of disease. *Parasitology* **137,** 755–772
5. Riley, E. M., Couper, K. N., Helmby, H., Hafalla, J. C., de Souza, J. B., Langhorne, J., Jarra, W. B., and Zavala, F. (2010) Neuropathogenesis of human and murine malaria. *Trends Parasitol.* **26,** 277–278
6. Medana, I. M., Hunt, N. H., and Chan-Ling, T. (1997) Early activation of microglia in the pathogenesis of fatal murine cerebral malaria. *Glia* **19,** 91–103
7. Rénia, L., Potter, S. M., Mauduit, M., Rosa, D. S., Kayibanda, M., Deschemin, J. C., Snounou, G., and Grüner, A. C. (2006) Pathogenic T cells in cerebral malaria. *Int. J. Parasitol* **36,** 547–554
8. Amante, F. H., Haque, A., Stanley, A. C., Rivera Fde, L., Randall, L. M., Wilson, Y. A., Yeo, G., Pieper, C., Crabb, B. S., de Koning-Ward, T. F., Lundie, R. J., Good, M. F., Pinzon-Charry, A., Pearson, M. S., Duke, M. G.,

McManus, D. P., Loukas, A., Hill, G. R., and Engwerda, C. R. (2010) Immune-mediated mechanisms of parasite tissue sequestration during experimental cerebral malaria. *J. Immunol.* **185,** 3632–3642
9. Patel, S. N., Serghides, L., Smith, T. G., Febbraio, M., Silverstein, R. L., Kurtz, T. W., Pravenec, M., and Kain, K. C. (2004) CD36 mediates the phagocytosis of Plasmodium falciparum-infected erythrocytes by rodent macrophages. *J. Infect. Dis.* **189,** 204–213
10. Ayi, K., Patel, S. N., Serghides, L., Smith, T. G., and Kain, K. C. (2005) Nonopsonic phagocytosis of erythrocytes infected with ring-stage Plasmodium falciparum. *Infect. Immun.* **73,** 2559–2563
11. Gazzinelli, R. T., Wysocka, M., Hieny, S., Scharton-Kersten, T., Cheever, A., Kühn, R., Müller, W., Trinchieri, G., and Sher, A. (1996) In the absence of endogenous IL-10, mice acutely infected with *Toxoplasma gondii* succumb to a lethal immune response dependent on $CD4^+$ T cells and accompanied by overproduction of IL-12, IFN-γ and TNF-α. *J. Immunol.* **157,** 798–805
12. Wolf, S. A., and Ullrich, O. (2008) Endocannabinoids and the brain immune system: new neurones at the horizon? *J. Neuroendocrinol.* **20,** 15–19
13. Cabral, G. A., and Griffin-Thomas, L. (2009) Emerging role of the cannabinoid receptor CB2 in immune regulation: therapeutic prospects for neuroinflammation. *Expert Rev. Mol. Med.* **11,** e3
14. Centonze, D., Rossi, S., Finazzi-Agrò, A., Bernardi, G., and Maccarrone, M. (2007) The (endo)cannabinoid system in multiple sclerosis and amyotrophic lateral sclerosis. *Int. Rev. Neurobiol.* **82,** 171–186
15. Ashton, J. C., Rahman, R. M., Nair, S. M., Sutherland, B. A., Glass, M., and Appleton, I. (2007) Cerebral hypoxia-ischemia and middle cerebral artery occlusion induce expression of the cannabinoid CB2 receptor in the brain. *Neurosci. Lett.* **412,** 114–117
16. Atwood, B. K., and Mackie, K. (2010) CB2: a cannabinoid receptor with an identity crisis. *Br. J. Pharmacol.* **160,** 467–479
17. Stella, N. (2010) Cannabinoid and cannabinoid-like receptors in microglia, astrocytes, and astrocytomas. *Glia* **58,** 1017–1030
18. Palazuelos, J., Aguado, T., Pazos, M. R., Julien, B., Carrasco, C., Resel, E., Sagredo, O., Benito, C., Romero, J., Azcoitia, I., Fernández-Ruiz, J., Guzmán, M., and Galve-Roperh, I. (2009) Microglial CB2 cannabinoid receptors are neuroprotective in Huntington's disease excitotoxicity. *Brain* **132,** 3152–3164
19. Racz, I., Nadal, X., Alferink, J., Baños, J. E., Rehnelt, J., Martín, M., Pintado, B., Gutierrez-Adan, A., Sanguino, E., Bellora, N., Manzanares, J., Zimmer, A., and Maldonado, R. (2008) Interferon-γ is a critical modulator of CB(2) cannabinoid receptor signaling during neuropathic pain. *J. Neurosci.* **28,** 12136–12145
20. Buckley, N. E., McCoy, K. L., Mezey, E., Bonner, T., Zimmer, A., Felder, C. C., Glass, M., and Zimmer, A. (2000) Immunomodulation by cannabinoids is absent in mice deficient for the cannabinoid CB(2) receptor. *Eur. J. Pharmacol.* **396,** 141–149
21. Chuchawankul, S., Shima, M., Buckley, N. E., Hartmann, C. B., and McCoy, K. L. (2004) Role of cannabinoid receptors in inhibiting macrophage costimulatory activity. *Int. Immunopharmacol.* **4,** 265–278
22. Correa, F., Mestre, L., Docagne, F., and Guaza, C. (2005) Activation of cannabinoid CB2 receptor negatively regulates IL-12p40 production in murine macrophages: role of IL-10 and ERK1/2 kinase signaling. *Br. J. Pharmacol.* **145,** 441–448
23. Ross, R. A., Brockie, H. C., and Pertwee, R. G. (2000) Inhibition of nitric oxide production in RAW264.7 macrophages by cannabinoids and palmitoylethanolamide. *Eur. J. Pharmacol.* **401,** 121–130
24. Kogan, N. M., and Mechoulam, R. (2007) Cannabinoids in health and disease. *Dialogues Clin. Neurosci.* **9,** 413–430
25. Baptista, F. G., Pamplona, A., Pena, A. C., Mota, M. M., Pied, S., and Vigário, A. M. (2010) Accumulation of *Plasmodium berghei*-infected red blood cells in the brain is crucial for the development of cerebral malaria in mice. *Infect. Immun.* **78,** 4033–4039
26. Pertwee, R. G. (2008) Ligands that target cannabinoid receptors in the brain: from THC to anandamide and beyond. *Addict. Biol.* **13,** 147–159
27. Amante, F. H., Stanley, A. C., Randall, L. M., Zhou, Y., Haque, A., McSweeney, K., Waters, A. P., Janse, C. J., Good, M. F., Hill, G. R., and Engwerda, C. R. (2007) A role for natural regulatory T cells in the pathogenesis of experimental cerebral malaria. *Am. J. Pathol.* **171,** 548–559
28. McQuillan, J. A., Mitchell, A. J., Ho, Y. F., Combes, V., Ball, H. J., Golenser, J., Grau, G. E., and Hunt, N. H. (2011) Coincident parasite and CD8 T cell sequestration is required for development of experimental cerebral malaria. *Int. J. Parasitol.* **41,** 155–163
29. Riley, E. M., and Stewart, V. A. (2013) Immune mechanisms in malaria: new insights in vaccine development. *Nat. Med.* **19,** 168–178
30. Haque, A., Best, S. E., Unosson, K., Amante, F. H., de Labastida, F., Anstey, N. M., Karupiah, G., Smyth, M. J., Heath, W. R., and Engwerda, C. R. (2011) Granzyme B expression by $CD8^+$ T cells is required for the development of experimental cerebral malaria. *J. Immunol.* **186,** 6148–6156
31. Hunt, N. H., and Grau, G. E. (2003) Cytokines: accelerators and brakes in the pathogenesis of cerebral malaria. *Trends Immunol.* **24,** 491–499
32. Gordon, S., and Martinez, F. O. (2010) Alternative activation of macrophages: mechanism and functions. *Immunity* **32,** 593–604
33. Mildner, A., and Jung, S. (2014) Development and function of dendritic cell subsets. *Immunity* **40,** 642–656
34. Hey, Y. Y., and O'Neill, H. C. (2012) Murine spleen contains a diversity of myeloid and dendritic cells distinct in antigen presenting function. *J. Cell. Mol. Med.* **16,** 2611–2619
35. Kastenmüller, W., Torabi-Parizi, P., Subramanian, N., Lämmermann, T., and Germain, R. N. (2012) A spatially organized multicellular innate immune response in lymph nodes limits systemic pathogen spread. *Cell* **150,** 1235–1248
36. Wu, X., Gowda, N. M., and Gowda, D. C. (2015) Phagosomal acidification prevents macrophage inflammatory cytokine production to malaria, and dendritic cells are the major source at the early stages of infection: implication for malaria protective immunity development. *J. Biol. Chem.* **290,** 23135–23147
37. Beyer, M., Mallmann, M. R., Xue, J., Staratschek-Jox, A., Vorholt, D., Krebs, W., Sommer, D., Sander, J., Mertens, C., Nino-Castro, A., Schmidt, S. V., and Schultze, J. L. (2012) High-resolution transcriptome of human macrophages. *PLoS One* **7,** e45466
38. Martinez, F. O., Helming, L., and Gordon, S. (2009) Alternative activation of macrophages: an immunologic functional perspective. *Annu. Rev. Immunol.* **27,** 451–483
39. Alferink, J., Lieberam, I., Reindl, W., Behrens, A., Weiss, S., Hüser, N., Gerauer, K., Ross, R., Reske-Kunz, A. B., Ahmad-Nejad, P., Wagner, H., and Förster, I. (2003) Compartmentalized production of CCL17 *in vivo*: strong inducibility in peripheral dendritic cells contrasts selective absence from the spleen. *J. Exp. Med.* **197,** 585–599
40. Specht, S., Frank, J. K., Alferink, J., Dubben, B., Layland, L. E., Denece, G., Bain, O., Förster, I., Kirschning, C. J., Martin, C., and Hoerauf, A. (2011) CCL17 controls mast cells for the defense against filarial larval entry. *J. Immunol.* **186,** 4845–4852
41. Jordà, M. A., Verbakel, S. E., Valk, P. J., Vankan-Berkhoudt, Y. V., Maccarrone, M., Finazzi-Agrò, A., Löwenberg, B., and Delwel, R. (2002) Hematopoietic cells expressing the peripheral cannabinoid receptor migrate in response to the endocannabinoid 2-arachidonoylglycerol. *Blood* **99,** 2786–2793
42. Ghosh, S., Preet, A., Groopman, J. E., and Ganju, R. K. (2006) Cannabinoid receptor CB2 modulates the CXCL12/CXCR4-mediated chemotaxis of T lymphocytes. *Mol. Immunol.* **43,** 2169–2179
43. Pereira, J. P., An, J., Xu, Y., Huang, Y., and Cyster, J. G. (2009) Cannabinoid receptor 2 mediates the retention of immature B cells in bone marrow sinusoids. *Nat. Immunol.* **10,** 403–411
44. Miller, A. M., and Stella, N. (2008) CB2 receptor-mediated migration of immune cells: it can go either way. *Br. J. Pharmacol.* **153,** 299–308
45. Besnard, A. G., Guabiraba, R., Niedbala, W., Palomo, J., Reverchon, F., Shaw, T. N., Couper, K. N., Ryffel, B., and Liew, F. Y. (2015) IL-33-mediated protection against experimental cerebral malaria is linked to induction of type 2 innate lymphoid cells, M2 macrophages and regulatory T cells. *PLoS Pathog.* **11,** e1004607
46. Bose, T. O., Pham, Q. M., Jellison, E. R., Mouries, J., Ballantyne, C. M., and Lefrançois, L. (2013) CD11a regulates effector CD8 T cell differentiation and central memory development in response to infection with *Listeria monocytogenes*. *Infect. Immun.* **81,** 1140–1151
47. Backer, R., Schwandt, T., Greuter, M., Oosting, M., Jüngerkes, F., Tüting, T., Boon, L., O'Toole, T., Kraal, G., Limmer, A., and den Haan, J. M. (2010)

Effective collaboration between marginal metallophilic macrophages and $CD8^+$ dendritic cells in the generation of cytotoxic T cells. *Proc. Natl. Acad. Sci. U.S.A.* **107,** 216–221
48. Mukhopadhyay, S., Plüddemann, A., and Gordon, S. (2009) Macrophage pattern recognition receptors in immunity, homeostasis and self tolerance. *Adv. Exp. Med. Biol.* **653,** 1–14
49. Kossodo, S., Monso, C., Juillard, P., Velu, T., Goldman, M., and Grau, G. E. (1997) Interleukin-10 modulates susceptibility in experimental cerebral malaria. *Immunology* **91,** 536–540
50. Youn, J. I., and Gabrilovich, D. I. (2010) The biology of myeloid-derived suppressor cells: the blessing and the curse of morphological and functional heterogeneity. *Eur. J. Immunol.* **40,** 2969–2975
51. Cripps, J. G., and Gorham, J. D. (2011) MDSC in autoimmunity. *Int. Immunopharmacol.* **11,** 789–793
52. Van Ginderachter, J. A., Beschin, A., De Baetselier, P., and Raes, G. (2010) Myeloid-derived suppressor cells in parasitic infections. *Eur. J. Immunol.* **40,** 2976–2985
53. Hegde, V. L., Nagarkatti, M., and Nagarkatti, P. S. (2010) Cannabinoid receptor activation leads to massive mobilization of myeloid-derived suppressor cells with potent immunosuppressive properties. *Eur. J. Immunol.* **40,** 3358–3371
54. Louvet, A., Teixeira-Clerc, F., Chobert, M. N., Deveaux, V., Pavoine, C., Zimmer, A., Pecker, F., Mallat, A., and Lotersztajn, S. (2011) Cannabinoid CB2 receptors protect against alcoholic liver disease by regulating Kupffer cell polarization in mice. *Hepatology* **54,** 1217–1226
55. Zarruk, J. G., Fernández-López, D., García-Yébenes, I., García-Gutiérrez, M. S., Vivancos, J., Nombela, F., Torres, M., Burguete, M. C., Manzanares, J., Lizasoain, I., and Moro, M. A. (2012) Cannabinoid type 2 receptor activation downregulates stroke-induced classic and alternative brain macrophage/microglial activation concomitant to neuroprotection. *Stroke* **43,** 211–219
56. Sponaas, A. M., Cadman, E. T., Voisine, C., Harrison, V., Boonstra, A., O'Garra, A., and Langhorne, J. (2006) Malaria infection changes the ability of splenic dendritic cell populations to stimulate antigen-specific T cells. *J. Exp. Med.* **203,** 1427–1433
57. Voisine, C., Mastelic, B., Sponaas, A. M., and Langhorne, J. (2010) Classical $CD11c^+$ dendritic cells, not plasmacytoid dendritic cells, induce T cell responses to *Plasmodium chabaudi* malaria. *Int. J. Parasitol.* **40,** 711–719
58. deWalick, S., Amante, F. H., McSweeney, K. A., Randall, L. M., Stanley, A. C., Haque, A., Kuns, R. D., MacDonald, K. P., Hill, G. R., and Engwerda, C. R. (2007) Cutting edge: conventional dendritic cells are the critical APC required for the induction of experimental cerebral malaria. *J. Immunol.* **178,** 6033–6037
59. Lundie, R. J., de Koning-Ward, T. F., Davey, G. M., Nie, C. Q., Hansen, D. S., Lau, L. S., Mintern, J. D., Belz, G. T., Schofield, L., Carbone, F. R., Villadangos, J. A., Crabb, B. S., and Heath, W. R. (2008) Blood-stage *Plasmodium* infection induces $CD8^+$ T lymphocytes to parasite-expressed antigens, largely regulated by $CD8\alpha^+$ dendritic cells. *Proc. Natl. Acad. Sci. U.S.A.* **105,** 14509–14514
60. Yañez, D. M., Manning, D. D., Cooley, A. J., Weidanz, W. P., and van der Heyde, H. C. (1996) Participation of lymphocyte subpopulations in the pathogenesis of experimental murine cerebral malaria. *J. Immunol.* **157,** 1620–1624
61. Potter, S., Chan-Ling, T., Ball, H. J., Mansour, H., Mitchell, A., Maluish, L., and Hunt, N. H. (2006) Perforin mediated apoptosis of cerebral microvascular endothelial cells during experimental cerebral malaria. *Int. J. Parasitol.* **36,** 485–496
62. Nitcheu, J., Bonduelle, O., Combadiere, C., Tefit, M., Seilhean, D., Mazier, D., and Combadiere, B. (2003) Perforin-dependent brain-infiltrating cytotoxic $CD8^+$ T lymphocytes mediate experimental cerebral malaria pathogenesis. *J. Immunol.* **170,** 2221–2228
63. Mebius, R. E., and Kraal, G. (2005) Structure and function of the spleen. *Nat. Rev. Immunol.* **5,** 606–616
64. Poppensieker, K., Otte, D. M., Schürmann, B., Limmer, A., Dresing, P., Drews, E., Schumak, B., Klotz, L., Raasch, J., Mildner, A., Waisman, A., Scheu, S., Knolle, P., Forster, I., Prinz, M., *et al.* (2012) CC chemokine receptor 4 is required for experimental autoimmune encephalomyelitis by regulating GM-CSF and IL-23 production in dendritic cells. *Proc. Natl. Acad. Sci. U.S.A.* **109,** 3897–3902
65. Sigel, E., Baur, R., Rácz, I., Marazzi, J., Smart, T. G., Zimmer, A., and Gertsch, J. (2011) The major central endocannabinoid directly acts at $GABA_A$ receptors. *Proc. Natl. Acad. Sci. U.S.A.* **108,** 18150–18155
66. Montecucco, F., Matias, I., Lenglet, S., Petrosino, S., Burger, F., Pelli, G., Braunersreuther, V., Mach, F., Steffens, S., and Di Marzo, V. (2009) Regulation and possible role of endocannabinoids and related mediators in hypercholesterolemic mice with atherosclerosis. *Atherosclerosis* **205,** 433–441
67. Capasso, R., Izzo, A. A., Fezza, F., Pinto, A., Capasso, F., Mascolo, N., and Di Marzo, V. (2001) Inhibitory effect of palmitoylethanolamide on gastrointestinal motility in mice. *Br. J. Pharmacol.* **134,** 945–950
68. Russo, R., Loverme, J., La Rana, G., Compton, T. R., Parrott, J., Duranti, A., Tontini, A., Mor, M., Tarzia, G., Calignano, A., and Piomelli, D. (2007) The fatty acid amide hydrolase inhibitor URB597 (cyclohexylcarbamic acid 3′-carbamoylbiphenyl-3-yl ester) reduces neuropathic pain after oral administration in mice. *J. Pharmacol. Exp. Ther.* **322,** 236–242
69. Specht, S., Arriens, S., and Hoerauf, A. (2006) Induction of chronic colitis in IL-10 deficient mice requires IL-4. *Microbes Infect.* **8,** 694–703